Experimental Investigations of Air Entrainment in Transition and Skimming Flows down a Stepped Chute

Application to Embankment Overflow Stepped Spillways

H. CHANSON (*Reader*) and L. TOOMBES (*Associate Lecturer*)

Dept of Civil Engineering, The University of Queensland, Brisbane QLD 4072, Australia

Fax : (61 7) 33 65 45 99

URL: http://www.uq.edu.au/~e2hchans

Email: h.chanson@mailbox.uq.edu.au

ABSTRACT: Stepped spillways have been used for about 3,500 years. The last few decades have seen the development of new construction materials, design techniques and applications : e.g., embankment overtopping protection systems. Although it is commonly acknowledged that free-surface aeration is significant in stepped chutes, experimental data are scarce, often limited to very steep slopes ($\alpha \sim 50°$). The paper presents an experimental study conducted in a large-size stepped chute ($\alpha = 22°$, h = 0.1 m, W = 1 m). Observations demonstrate the existence of a transition flow pattern for intermediate flow rates between nappe and skimming flows. Detailed air-water flow measurements were conducted in both transition and skimming flows, immediately downstream of the inception point of free-surface aeration where uniform equilibrium flow conditions were not achieved. In skimming flows, a complete characterisation is developed for the distributions of void fraction, bubble count rate and velocity, and flow resistance is estimated including drag reduction effects. Transition flows exhibit significantly different air-water flow properties. They are highly aerated, requiring the design of comparatively high chute sidewalls. The design of embankment overflow stepped spillway is discussed in the light of the new results and design recommendations are provided. Major design issues include the step stability at the plunge point for high tailwater levels, the interactions between free-surface and seepage flows which could lead to further drag reduction, and secondary currents at the connection between steps and abutments.

Keywords : stepped spillway, air entrainment, two-phase flow properties, drag reduction, embankment overflow protection.

Table of contents

Notation

a   air-water specific area (1/m);

a_{mean} depth-averaged air-water specific area (1/m);

C   air concentration defined as the volume of air per unit volume, also called void fraction;

C_{mean} depth averaged air concentration defined as : $(1 - Y_{90}) * C_{mean} = d$;

C_p inflow pressure coefficient defined as :

$$C_p = \frac{1}{\frac{1}{2} * \rho * g * d^2} * \int_0^d P(y) * dy$$

D_H hydraulic diameter (m); $D_H = 4*d*W/(W + 2*d)$ for a rectangular channel;

D_t turbulent diffusivity (m^2/s) of air bubble in air-water flows;

D_o dimensionless coefficient;

D'   dimensionless air bubble diffusivity (defined by CHANSON 1995b);

d   1- flow depth measured normal to the channel slope at the edge of a step;

           2- characteristic depth (m) defined as : $d = \int_0^{Y_{90}} (1 - C) * dy$;

           3- channel height (m);

d_c critical flow depth (m); for a rectangular channel : $d_c = \sqrt[3]{q_w^2/g}$;

d_o inflow depth (m);

F_{ab} bubble count rate (Hz) : i.e., number of bubbles detected by the probe sensor per second;

$(F_{ab})_{max}$ maximum bubble count rate (Hz);

F_{ej} average cavity ejection frequency (Hz);

f   Darcy friction factor for water flows;

f_d equivalent Darcy friction factor estimate of the form drag;

f_e Darcy friction factor of air-water flows

f_i Darcy friction factor, neglecting air entrainment;

g   gravity constant (m/s^2) or acceleration of gravity; g = 9.80 m/s^2 in Brisbane;

H   total head (m);

h   height of steps (m) (measured vertically);

k   Von Karman constant;

K	inverse of the spreading rate of a turbulent shear layer;
K'	integration constant;
K^*	$K^* = \tanh^{-1}(\sqrt{0.1}) = 0.32745015...;$
k_s	cavity depth (m) (or roughness height);
L_{cav}	cavity length (m), or step cavity length (m) measured between step edges;
l	horizontal length of steps (m) (measured perpendicular to the vertical direction);
N	exponent of the velocity power law;
n	exponent;
P	pressure (Pa);
Q	discharge (m^3/s);
q	discharge per unit width (m^2/s);
R	normalised cross-correlation coefficient;
S_f	friction slope;
s	curvi-linear coordinate (m) measured in the flow direction
T	bubble travel time (s) for which the cross-correlation function is maximum;
Tu	turbulence intensity defined as : $Tu = u'/V$;
Tu'	characteristic turbulence intensity in air-water flows (App. IV);
t, t'	time (s);
U_w	clear-water flow velocity (m/s) : $U_w = q_w/d$;
u'	root mean square of longitudinal component of turbulent velocity (m/s);
u_r	bubble rise velocity (m/s);
$(u_r)_{Hyd}$	bubble rise velocity (m/s) in a hydrostatic pressure gradient;
V	velocity (m/s);
V_c	critical velocity (m/s); for a rectangular channel : $V_c = \sqrt[3]{g * q_w}$;
V_{90}	characteristic velocity (m/s) where the air concentration is 90%;
V_o	free-stream velocity (m/s);
W	channel width (m);
x	longitudinal distance (m);
Y_{90}	characteristic depth (m) where the air concentration is 90%;

y   1- distance (m) from the bottom measured perpendicular to the spillway invert;

2- distance (m) from the pseudo-bottom (formed by the step edges) measured perpendicular to the flow direction;

Greek symbols

α channel slope;

Δx distance between probe sensors (m);

δx characteristic sensor size (m) in the flow direction;

δ_{BL} boundary layer thickness (m);

δ_* displacement thickness (m);

δ_M momentum thickness (m);

λ dimensionless coefficient;

μ dynamic viscosity (N.s/m^2);

ν kinematic viscosity (m^2/s);

π $\pi = 3.141592653589793238462643...$;

ρ density (kg/m^3);

σ surface tension between air and water (N/m);

τ_o boundary shear stress (Pa);

$\varnothing$ diameter (m);

Subscript

air   air flow;

c   critical flow conditions;

w   water flow;

Abbreviations

RCC   roller compacted concrete.

About the writers

Hubert Chanson received a degree of 'Ingénieur Hydraulicien' from the Ecole Nationale Supérieure d'Hydraulique et de Mécanique de Grenoble (France) in 1983 and a degree

Atomique' from the 'Institut National des Sciences et Techniques Nucléaires' in 1984. He worked for the industry in France as a R&D engineer at the Atomic Energy Commission from 1984 to 1986, and as a computer professional in fluid mechanics for Thomson-CSF between 1989 and 1990. From 1986 to 1988, he studied at the University of Canterbury (New Zealand) as part of a Ph.D. project. He was awarded a Doctor of Engineering from the University of Queensland in 1999 for outstanding research achievements in gas-liquid bubbly flows.

Hubert Chanson is a reader in environmental fluid mechanics and water engineering at the University of Queensland since 1990. His research interests include design of hydraulic structures, experimental investigations of two-phase flows, coastal hydrodynamics, water quality modelling, environmental management and natural resources. He is the author of four books : "Hydraulic Design of Stepped Cascades, Channels, Weirs and Spillways" (*Pergamon*, 1995), "Air Bubble Entrainment in Free-Surface Turbulent Shear Flows" (*Academic Press*, 1997), "The Hydraulics of Open Channel Flows : An Introduction" (*Butterworth-Heinemann*, 1999) and "The Hydraulics of Stepped Chutes and Spillways" (*Balkema*, 2001). His publication record includes over 180 international refereed papers and his work was cited over 600 times since 1990. Hubert Chanson has been active also as consultant for both governmental agencies and private organisations. He has been awarded five fellowships from the Australian Academy of Science. In 1995 he was a Visiting Associate Professor at National Cheng Kung University (Taiwan R.O.C.) and he was Visiting Research Fellow at Toyohashi University of Technology (Japan) in 1999 and 2001.

Hubert Chanson was the keynote lecturer at the 1998 ASME Fluids Engineering Symposium on Flow Aeration (Washington DC), at the Workshop on Flow Characteristics around Hydraulic Structures (Nihon University, Japan 1998) and at the first International Conference of the International Federation for Environmental Management System IFEMS'01 (Tsurugi, Japan 2001). He gave an invited lecture at the International Workshop on Hydraulics of Stepped Spillways (ETH-Zürich, 2000). He lectured several short courses in Australia and overseas (e.g. Taiwan).

Luke Toombes graduated a Bachelor in Civil Engineering (BEng., 1st Hon.) at the University of Queensland in 1994. He worked for the industry in Australia from 1995 to 1996 as a consulting engineer for Cullen, Grummitt & Roe Pty Ltd, with expertise in the design and management of ports and harbours, both in Australia and overseas. Between 1996 and 2001, he studied at the University of Queensland as part of a Ph.D. project investigating the air-water flow properties of stepped cascades. Luke Toombes is an Associate Lecturer in fluid mechanics at the Department of Civil Engineering, the University of Queensland. His research interests include coastal processes, hydraulic engineering and hydraulic structures. His publication record includes 10 international refereed papers and two refereed research reports. His work was cited more than 10 times since 1997.

Part I - Experimental investigations in a 1V:2.5H stepped spillway model

1. Introduction

Stepped spillways have been used for about 3,500 years (CHANSON 2000,2001). During the 19th century, the design technique was common in Europe, North-America and Australia (e.g. SCHUYLER 1909, WEGMANN 1911, KELEN 1933, CHANSON 1997a) (Fig. 1-1A). By the end of the 19th century, it was understood that stepped chutes contributed significantly to the dissipation of the flow energy : e.g., the design of the Gold Creek and New Croton dam spillways (WEGMANN 1907, CHANSON and WHITMORE 1998). The interest in stepped cascades dropped however during the first half of the 20th century with new progresses in the energy dissipation characteristics of hydraulic jumps favouring the design of hydraulic jump stilling basins. Stilling basins allowed larger energy dissipation and smaller structures, leading to cheaper construction costs.

Fig. 1-1 - Photographs of stepped spillways
(A) Pas du Riot dam, Planfroy, France in June 1998 - Completed in 1873 (H = 36 m), design discharge : 65 m^3/s, 7 steps (h ~ 2.5 à 3 m), trapezoidal cross-section (base width ~ 3 m)

Since the 1970s, the regain of interest for the stepped spillway design has been associated with the development of new construction materials (e.g. roller compacted concrete RCC, polymer coated gabions), the introduction of new design techniques (e.g. overflow embankment dam protection systems with RCC and precast concrete blocks), and the development of new applications (e.g. re-oxygenation cascades) (Fig. 1-1B). Research on stepped chute hydraulics has been very active : i.e., one book, sixteen journal papers and twenty-six discussions listed in Global Books in Print™ and Science Citation Index™ for the period 1985-2000. However most studies prior to 1992 neglected the effects of free-surface aeration ('white waters'), until the first data by RUFF and FRIZELL (1994) and the analysis of CHANSON (1993a). Today experimental data on air entrainment down stepped chute are scarce, often limited to very steep slopes ($\alpha \sim 50°$) as used for gravity dams (Table 1-1).

Table 1-1 - Detailed experimental investigations of air entrainment in stepped chutes

Reference	α deg.	q_w m²/s	h m	Flow regime	Remarks
(1)	(2)	(3)	(4)	(5)	(6)
CHANSON and TOOMBES (1997, 2000)	3.4	0.038 to 0.163	0.143	Nappe flow	W = 0.5 m. Supercritical inflow (0.03-m nozzle thickness).
TOZZI et al. (1998)	52.2	0.23	0.053	Skimming flow	Inflow: uncontrolled smooth WES ogee crest followed by smaller first steps.
CHAMANI and RAJARATNAM (1999)	51.3 & 59	0.07 to 0.2	0.313 to 0.125	Skimming flow	W = 0.30 m. Inflow: un-controlled smooth WES ogee crest.
MATOS (2000)	53.1	0.08 to 0.2	0.08	Skimming flow	W = 1 m. Inflow: uncontrolled WES ogee crest, with small first steps built in the ogee development.
TOOMBES and CHANSON (2000)	3.4	0.08 to 0.136	0.143	Nappe flow	W = 0.25 m. Supercritical inflow (nozzle thickness : 0.028 to 0.040 m). Ventilated steps.
BOES (2000)	30 & 50	--	0.023 to 0.09	Skimming flow	W = 0.5 m. Inflow: pressurised intake.
OHTSU et al. (2000)	55	0.016 to 0.03	0.025	Skimming flow	W = 0.3 m. Inflow: uncontrolled broad-crest.
Present study	21.8	0.04 to 0.18	0.1	Transition & Skimming flows	W = 1 m. Inflow: uncontrolled broad-crest.

Fig. 1-1 - Photographs of stepped spillways
(B) Riou dam, France in November 1994 - Completed in 1990 (H = 22 m), design discharge : 1.5 m^2/s, width : 96 m, h = 0.43 m, RCC construction

It is the purpose of this study to provide a comprehensive database on air-water flows down stepped chutes. Measurements were conducted on a large facility (h = 0.1 m, W = 1 m) with a precise instrumentation. (Based upon a Froude similitude, the large size of the facility ensures that the experimental results may be extrapolated to prototype with negligible scale effects for geometric scaling ratios less than 10:1.) Two flow regimes were investigated, providing a broad spectrum of flow conditions. A complete characterisation of the air-water flow properties is provided. The results are discussed in the context of embankment overflow stepped spillways and design recommendations are provided.

2. Experimental apparatus and instrumentation

Experiments were conducted at the University of Queensland in a 2.7-m long, 1-m wide, 21.8° slope chute (Table 2-1). Waters were supplied from a large feeding basin (1.5-m deep, surface area 6.8 m × 4.8 m) leading to a sidewall convergent with a 4.8:1 contraction ratio. The test section consisted of a broad-crested weir (1-m wide, 0.6-m long, with upstream rounded corner (0.057-m radius)) followed by nine identical steps (h = 0.1 m, l = 0.25 m) made of marine ply. The stepped chute was 1-m wide with

perspex sidewalls, followed by a horizontal concrete-invert canal ending in a dissipation pit.

Fig. 2-1 - Definition sketch of the test section
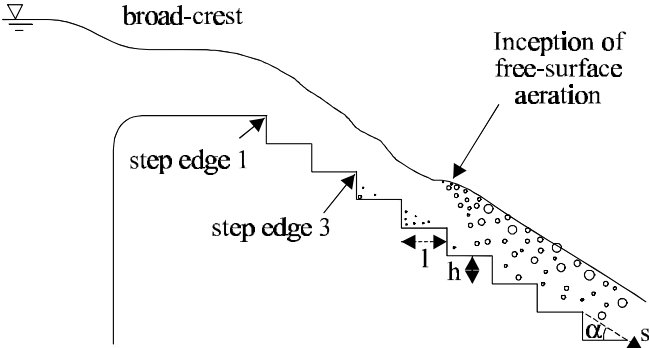
Table 2-1 - Summary of experimental flow conditions

Ref.	Q_W m^3/s	Location of inception of free-surface aeration	Flow regime	Remarks
(1)	(2)	(3)	(4)	(5)
Series 1				Single-tip probe
	0.182	Step edge 6	Skimming flow	Run Q5
	0.164	Step edge 6	Skimming flow	Run Q6
	0.147	Step edge 5	Skimming flow	Run Q7
	0.130	Step edge 5	Skimming flow	Run Q8
	0.124	Step edge 5	Skimming flow	Run Q1
	0.114	Step edge 5	Skimming flow	Run Q9
	0.103	Step edge 4	Skimming flow	Run Q2
	0.099	Step edge 4	Transition flow	Run Q10
	0.085	Step edge 4	Transition flow	Run Q11
	0.080	Step edge 4	Transition flow	Run Q3
	0.071	Step edge 3	Transition flow	Run Q12
	0.066	Step edge 3	Transition flow	Run Q4
	0.064	Step edge 3	Transition flow	Run Q13
	0.058	Step edge 3	Transition flow	Run Q14
	0.052	Step edge 3	Transition flow	Run Q15
	0.046	Step edge 3	Transition flow	Run Q16
Series 2				Double-tip probe
	0.182	Step edge 6	Skimming flow	Run Q23.
	0.114	Step edge 5	Skimming flow	Run Q21.
	0.058	Step edge 3	Transition flow	Run Q22.

The flow rate was delivered by a pump controlled with an adjustable frequency AC motor drive, enabling an accurate discharge adjustment in a closed-circuit system. The discharge was measured from the upstream head above crest with an accuracy of about 2% (ACKERS et al. 1978, BOS 1976). Clear-water flow depths and velocities were measured with a point gauge and a Prandtl-Pitot tube ($\varnothing$ =

3.3 mm) respectively. Air-water flow properties were measured using two types of conductivity probe: a single-tip probe ($\varnothing$ = 0.35 mm), and a double-tip probe ($\varnothing$ = 0.025 mm). The probe sensors were aligned in the flow direction and excited by an air bubble detector (AS25240). (The velocity measurements were the longitudinal component of the air-water interfacial velocity.) The probe signal was scanned at 5 kHz for 180 s and at 20 kHz for 20 s for the single-tip and double-tip probes respectively. The translation of the probes in the direction normal to the channel invert was controlled by a fine adjustment travelling mechanism connected to a Mitutoyo™ digimatic scale unit (Ref. No. 572-503). The error on the vertical position of the probe was less than 0.025 mm. The accuracy on the longitudinal position of the probe was estimated as $\Delta x < +/- 0.5$ cm. The accuracy on the transverse position of the probe was less than 1 mm. Flow visualisations were conducted with a digital video-camera Sony™ DV-CCD DCR-TRV900 (speed: 25 fr/s, shutter: 1/4 to 1/10,000 s) and high-speed still photographs.

Air-water flow properties were recorded for nineteen flow rates ranging from 0.046 to 0.182 m^3/s (Table 2-1). Measurements were conducted at the step edges, unless indicated (Fig. 2-1). Note that uniform equilibrium flow conditions were not achieved at the downstream end of the chute because the flume was relatively short. Full details of the experimental results are given in Appendix I.

3. Basic flow patterns

3.1 Flow regime

The facility was designed to operate with flow conditions ranging from nappe to skimming flow regimes (Fig. 3-1). For $d_c/h < 0.53$, where d_c is the critical depth and h is the step height, the water flowed down the chute as a succession of clear, distinct free-falling nappes (i.e. nappe flow regime). (Nappe flows were not specifically investigated. Relevant references include HORNER (1969) and CHANSON (1995a).) For $d_c/h > 0.97$, the flow skimmed over the pseudo-bottom formed by the step edges : i.e., skimming flow regime. Intense cavity recirculation was observed at each and every step. For intermediate discharges ($0.53 < d_c/h < 0.97$), a transition flow pattern was observed. Dominant flow features of transitions flows included strong splashing and droplet ejections at any position downstream of the inception point of free-surface aeration. Small to medium air cavities were observed irregularly. For example, a step with a small air pocket could be followed by a medium-size air cavity at the

downstream step, followed by a tiny air cavity at the next drop. For an observer standing on the bank, the transition flow had a chaotic appearance with irregular droplet ejections that were seen to reach heights of up to 3 to 5 times the step height. It did not have the quasi-smooth free-surface appearance of skimming flows, nor the distinctive succession of free-falling nappes observed in nappe flows.

With both transition and skimming flows, the upstream flow was non-aerated and the free-surface exhibited an undular profile of same wave length and in phase with the stepped invert profile. Free-surface instabilities were however observed (Fig. 3-2). Similar wave instabilities were discussed by ANWAR (1993) and CHANSON (1997b). ANWAR suggested that free-surface aeration may be initiated by free-surface wave development, while CHANSON showed experimental evidence of free-surface aeration in partially-developed flows.

The location of the inception of free-surface aeration was clearly defined for each and every test. (Experimental observations are reported in Table 2-1 & Appendix I.) Cavity aeration was typically observed one to two steps upstream of the inception point (Fig. 3-2). A similar observation was reported by HORNER (1969), CHAMANI (2000) and MATOS (2000).

Fig. 3-1 - Views of the experimental test section
(A) Skimming flow ($d_c/h = 1.5$) - Flow from left to right

(B) Transition flow ($d_c/h = 0.7$) - Photograph with high shutter speed (1/2,000 sec.)

Fig. 3-2 - Flow patterns next to the inception point of free-surface aeration
(A) Free-surface instabilities upstream of the inception point of free-surface aeration
Skimming flow, looking downstream ($d_c/h = 1.16$)
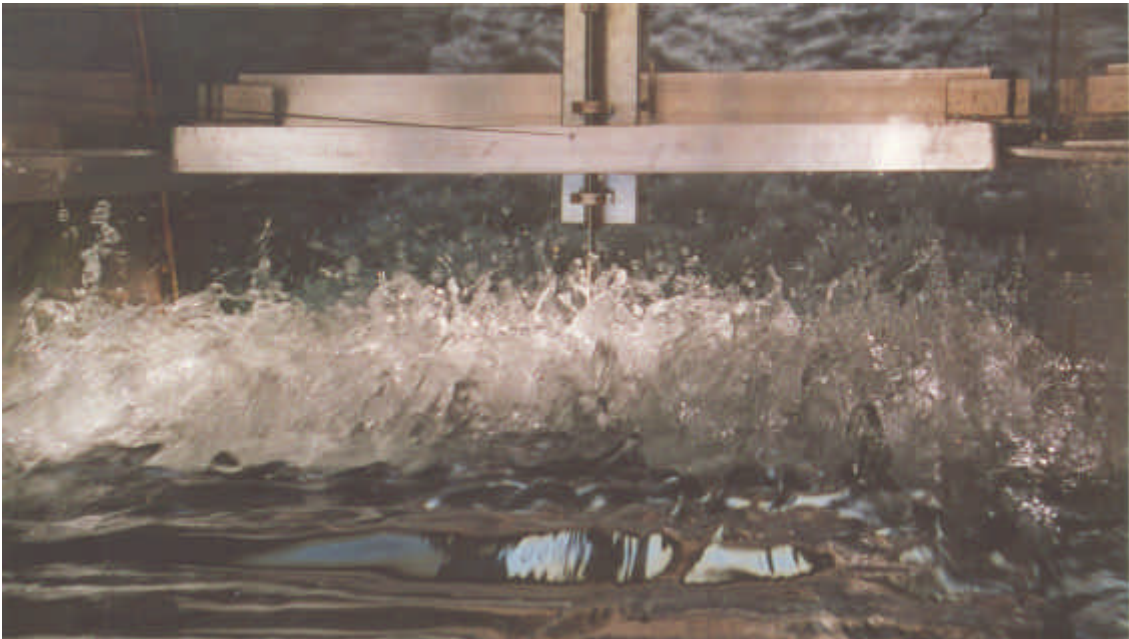
(B) Cavity aeration at the inception point of free-surface aeration (Courtesy of M. EASTMAN)
Transition flow, flow direction from the left to the right ($d_C/h = 0.6$) - Note the small air cavity
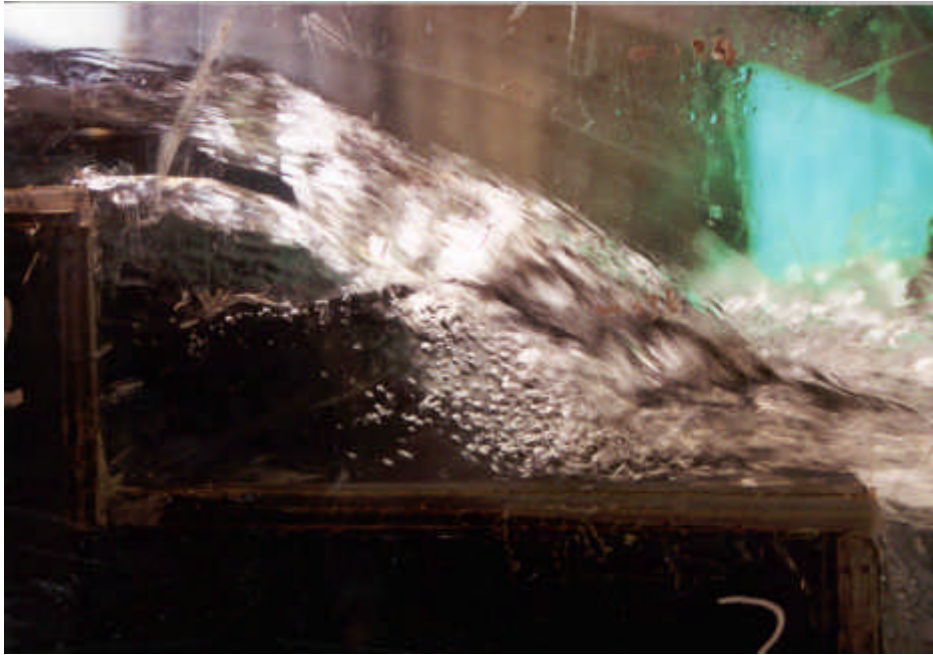
OHTSU and YASUDA (1997) were the first to mention the existence of a distinct "transition flow" regime (between nappe and skimming flows). The present observations of changes in flow regime are close to their findings : i.e., $0.78 < d_C/h < 1.05$ for $\alpha = 18.4°$ (YASUDA and OHTSU 1999). These are further consistent with previous reviews of nappe-to-skimming flow transition conditions (e.g. RAJARATNAM 1990, CHANSON 1996).

3.2 Cavity recirculation in skimming flows

In skimming flows, intense three-dimensional cavity recirculation was observed at each step for all flow rates (Table 2-1). The recirculation vortices were best observed next to and downstream of the inception point, where entrained air bubbles within the step cavity enhanced visualisation. The skimming flows were characterised by unsteady momentum exchanges between the main stream and cavity flows. The recirculating fluid, at irregular time intervals, flowed outward into the main flow and was replaced by fresh fluid (Fig. 3-3). The ejection mechanism appeared sequential. Once one cavity outflow occured, it induced a sequence of outflows at the downstream cavities. Figure 3-3 illustrates the sequential fluid ejection in three successive step cavities. (The time scale between the upper and lower sketch is typically very short.) A similar pattern was documented with skimming flows past strip

roughness ([1]) while the sequential fluid ejection process was observed on the M'Bali stepped spillway model by Professor LEJEUNE, and at Nihon University by Professor OHTSU and Dr YASUDA. This is discussed in Appendix II.

Energy considerations show that the average fluid ejection frequency F_{ej} is proportional to the dimensionless boundary shear stress, and that the average outflow velocity is about half of the fluid inflow velocity (Appendix II). For a wide chute with flat horizontal steps, the dimensionless cavity ejection frequency is of the order of magnitude of :

$$\frac{F_{ej} * (h*\cos\alpha)}{U_w} \sim \frac{f}{5} \qquad\qquad (3\text{-}1)$$

where U_w is the main flow velocity, f is the Darcy friction factor, h is the step height and α is the slope of the pseudo-invert formed by the step edges. The duration of fluid ejection (or burst) must be smaller than the average ejection period. This yields a limiting condition in terms of flow resistance : $f \leq 1$. Larger flow resistance implies that the flow energy is dissipated by further means other than viscous dissipation in the cavity recirculation.

4. Air-water flow properties in skimming flows

Basic air-water flow properties

Downstream of the inception point of free-surface aeration, a rapid free-surface aeration was observed. Air concentration distributions, measured at step edges, exhibited a smooth continuous profile. Experimental results are presented in Figure 4-1 and compared with an analytical solution of the air bubble advective diffusion equation :

$$C = 1 - \tanh^2\left(K'' - \frac{\dfrac{y}{Y_{90}}}{2*D_o} + \frac{\left(\dfrac{y}{Y_{90}} - \dfrac{1}{3}\right)^3}{3*D_o} \right) \qquad \text{Skimming flows (4-1)}$$

where y is distance measured normal to the pseudo-invert, Y_{90} is the characteristic distance where $C = 90\%$, K'' is an integration constant and D_o is a function of the mean air concentration C_{mean} only (App. III).

---

[1]Rectangular cavity : DJENEDI et al. (1994), ELAVARASAN et al. (1995). Triangular cavity : TANTIRIDGE et al. (1994).

Fig. 3-3 Sketch of sequential fluid ejections
From top to bottom : successive cavity ejections (burst and outflow) in three adjacent cavities
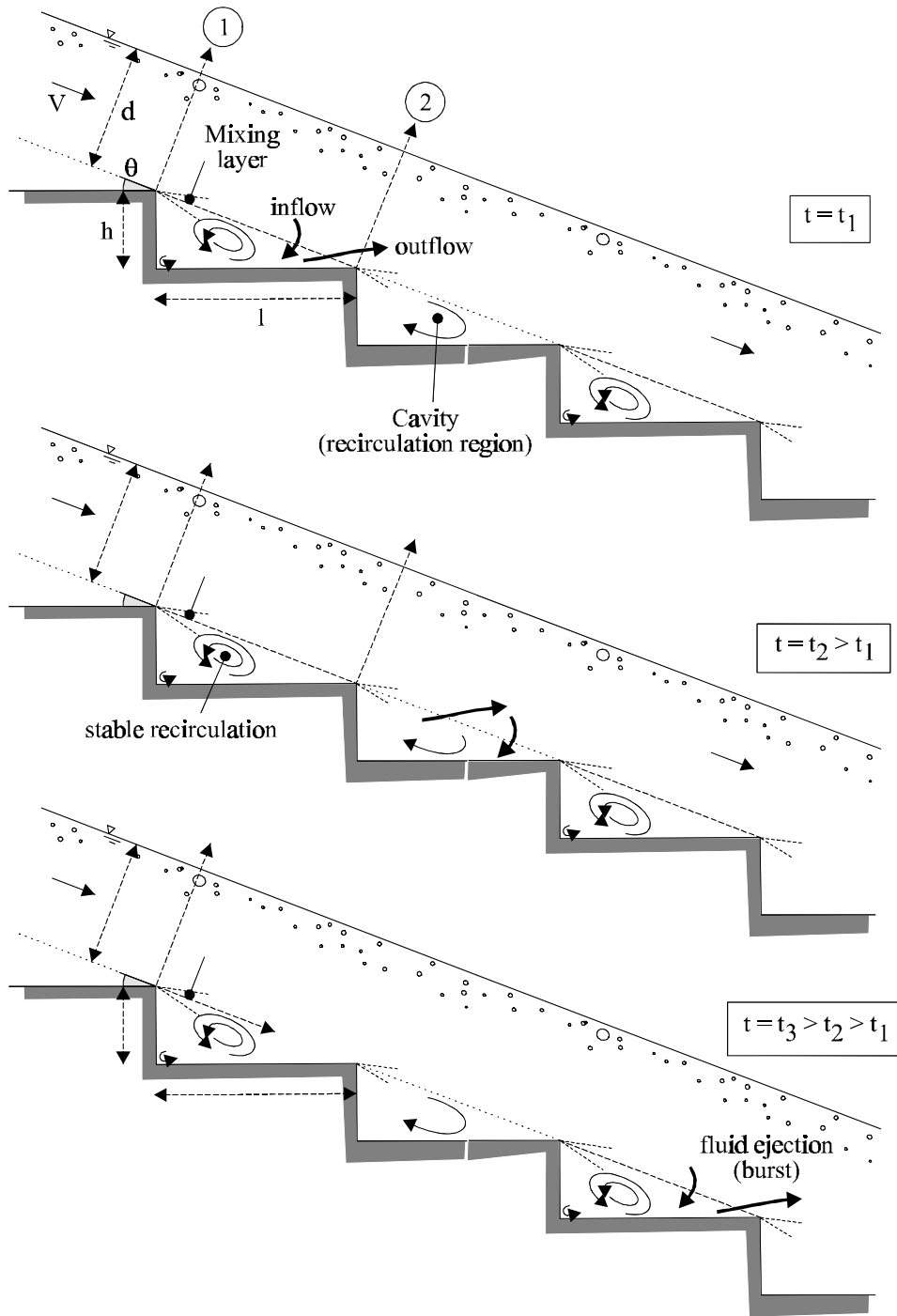
A small number of measurements were taken half-distance between two step edges (e.g. Fig. 4-1A). The

results suggest consistently a greater overall aeration than at adjacent step edges, with some aeration of

the fluid layers next to the recirculation cavity (i.e. $y/Y_{90} < 0.3$).

Velocity distributions measurements were performed at step edges (Fig. 4-1A). The results follow a

power law :

$$\frac{V}{V_{90}} = \left(\frac{y}{Y_{90}}\right)^{1/N} \tag{4-2}$$

where V_{90} is the characteristic velocity for C = 90%. N was found to be about 5.1 and 6 for d_c/h = 1.5 and 1.1 respectively. MATOS (2000) performed air-water velocity measurements in a longer chute and he observed N ~ 4. CHANSON (1995a) found N = 3.5 and 4 for the earlier works of FRIZELL (1992) and TOZZI (1992) respectively.

In the present study, the flume was relatively short and uniform equilibrium flow conditions were not achieved. This might account for some difference with MATOS' results.

Figure 4-1C presents dimensionless distributions of bubble count rates $F_{ab}*d_c/V_c$, where F_{ab} is the bubble frequency, d_c is the critical depth and V_c is the critical flow velocity. For a given flow velocity and void fraction, the bubble count rate F_{ab} is inversely proportional to the mean bubble size, and directly proportional to the air-water specific interface area (e.g. CHANSON 1997c). The relationship between the bubble frequency and air content exhibits a characteristic parabolic shape which is best fitted by :

Fig. 4-1 - Air-water flow properties in skimming flows
(A) Experimental data for $Q_w = 0.182$ m^3/s - Comparison with Equations (4-1) and (4-2)
Inception of free-surface aeration upstream of step edge 6
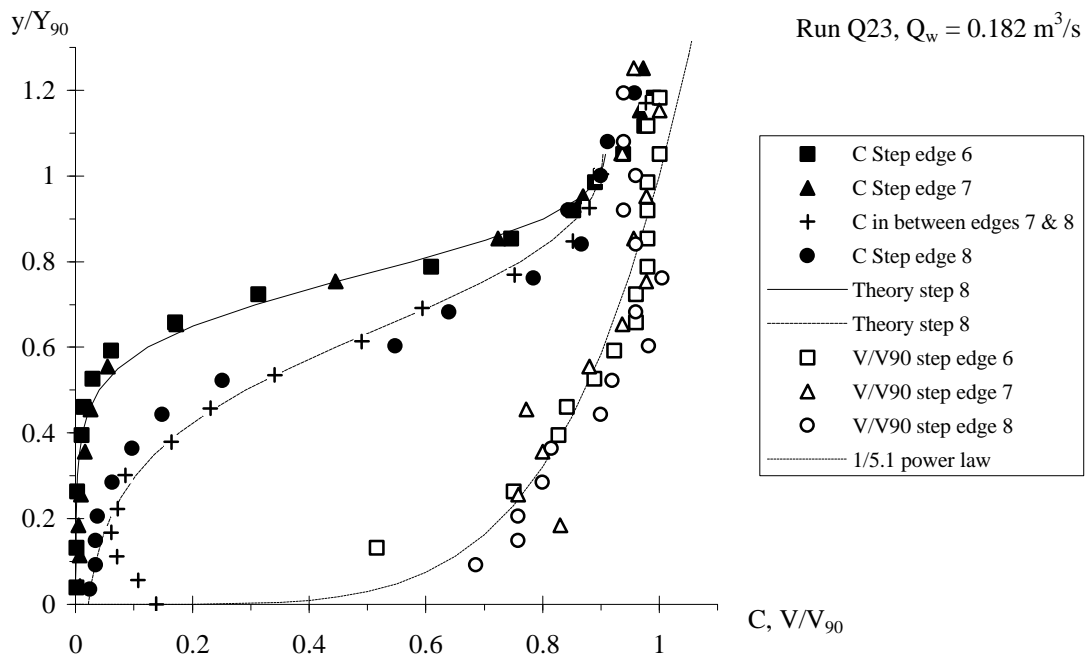
(B) Experimental data for $Q_W = 0.147$ m^3/s - Comparison with Equation (4-1)
Inception of free-surface aeration upstream of step edge 5
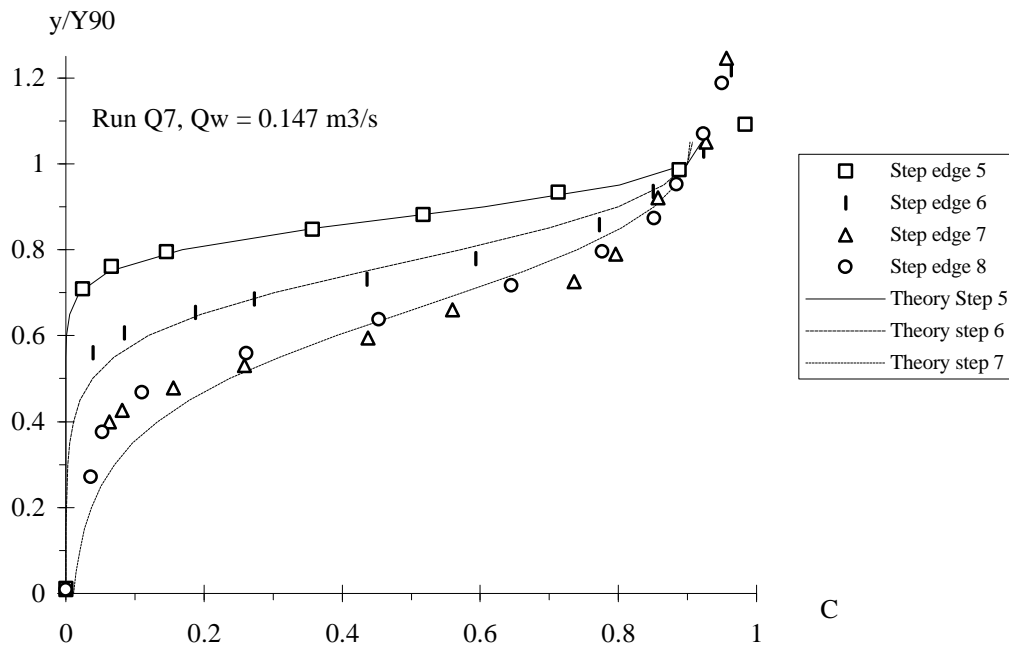
(C) Dimensionless bubble count rate distributions (data measured with single-tip probe) for $Q_W = 0.147$ m^3/s
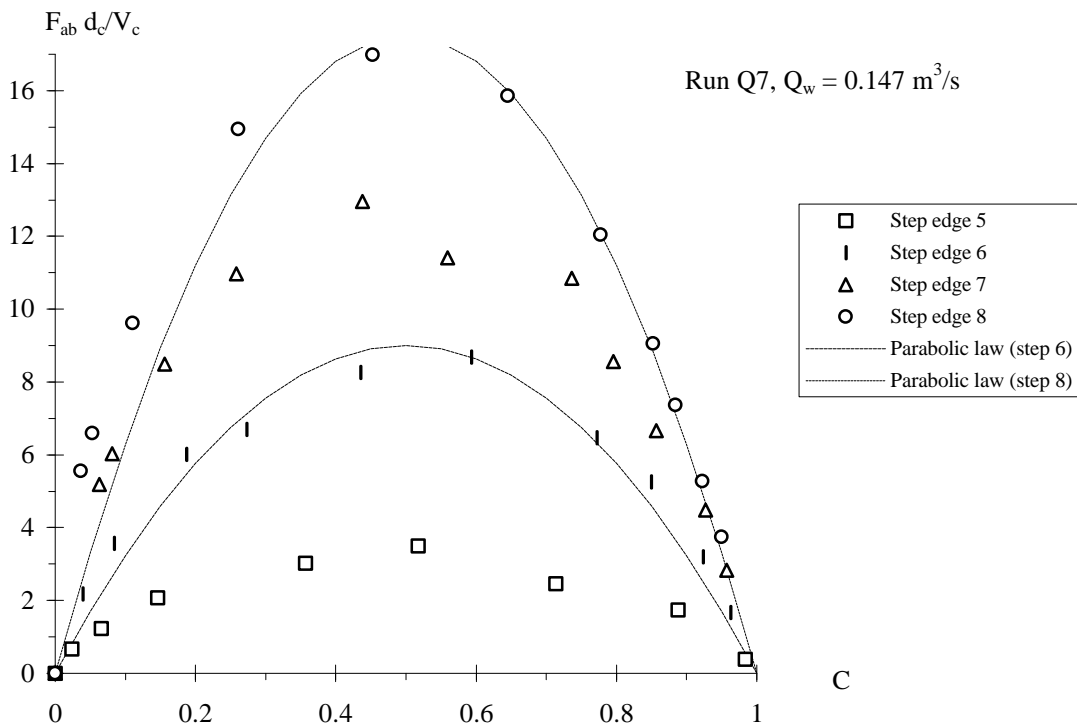
$$\frac{F_{ab}}{(F_{ab})_{max}} = 4 * C * (1 - C) \qquad\qquad (4\text{-}3)$$

where the maximum bubble frequency $(F_{ab})_{max}$ is seen for about $C \sim 50\%$.

Bubble and droplet chord length data

Measured chord length size distributions are presented in Figure 4-2. Each figure shows the normalised chord length probability distribution function where the histogram columns represent the probability of a bubble chord length in 0.5 mm intervals : e.g., the probability of a chord length from 2.0 to 2.5 mm is represented by the column labelled 2.0. The last column (i.e. > 20) indicates the probability of bubble chord lengths larger than 20 mm. Air bubble chord length distributions are in white and water droplet chord length distributions are in black. The data give some information on the characteristic sizes of air bubbles and water droplets. They show the broad spectrum of bubble and droplet chord lengths observed at each location : i.e., from less than 0.5 mm to larger than 20 mm (Fig. 4-2). Results from both the bubbly flow region (C < 0.3 to 0.4) and the splashing region (0.6 to 0.8 < C) are shown.

The air bubble chord length distributions are skewed with a preponderance of small bubble sizes relative to the mean. The probability of bubble chord lengths is the largest for bubble sizes between 0 and 1.5 mm for $C \approx 0.1$ and between 0 and 2.5 mm for $C \approx 0.2$. It is worth noting the large fraction of bubbles larger than 20 mm for $C \approx 10$ and 20%. These might be large air packets surrounding water structures. For completeness, the fraction of bubbles larger than 20 mm was significantly higher between step edges, possibly as the results of cavity aeration.

Although water droplet chord length distributions appeared skewed with a preponderance of small drop sizes relative to the mean, the distributions differ from bubble chord length distributions for similar liquid and void fractions respectively, indicating consistently larger droplet chord lengths (Fig. 4-2). A similar result was noted in smooth-invert chute flow (CHANSON 1999a).

Dimensionless specific interface area distributions were calculated. Results are presented in Appendix I in terms of the depth-averaged specific interface area a_{mean}. Experimental results show maximum specific interface areas up to 650 m^{-1}, with depth-average mean specific area ranging from 20 to 310 m^{-1} (App. I). For all skimming flow experiments, greater specific interface areas were measured in between step edges than at the adjacent step edges. It is believed that the aeration of the recirculation

flow contributes even further to the interface area ([2]).

Fig. 4-2 Bubble and droplet chord length distributions (white = air bubbles - black = water droplets)
(A) Void and liquid fractions : 10% ($Q_W = 0.182$ m^3/s)

	Y_{90} (m)	C_{mean}	$(F_{ab})_{max}$ (Hz)
Step edge 7	0.070	0.23	110
between step edges 7 and 8	0.090	0.40	123
Step edge 8	0.088	0.38	132

Probability

Run Q23, d_c/h=1.5, Step edge 7

□ C=0.06, y/Y90=0.55, 796 bubbles
■ C=0.94, y/Y90=1.05, 782 droplets

chord length size (mm)

Probability

Run Q23, between step edges 7 & 8

□ C=0.09, y/Y90=0.30, 1043 air bubbles
■ C=0.90, y/Y90=1.0, 1152 water droplets

chord length size (mm)

Probability

Run Q23, Step edge 8

□ C=0.10, y/Y90=0.36, 1661 air bubbles
■ C=0.9, y/Y90=1, 1185 water droplets

chord length size (mm)
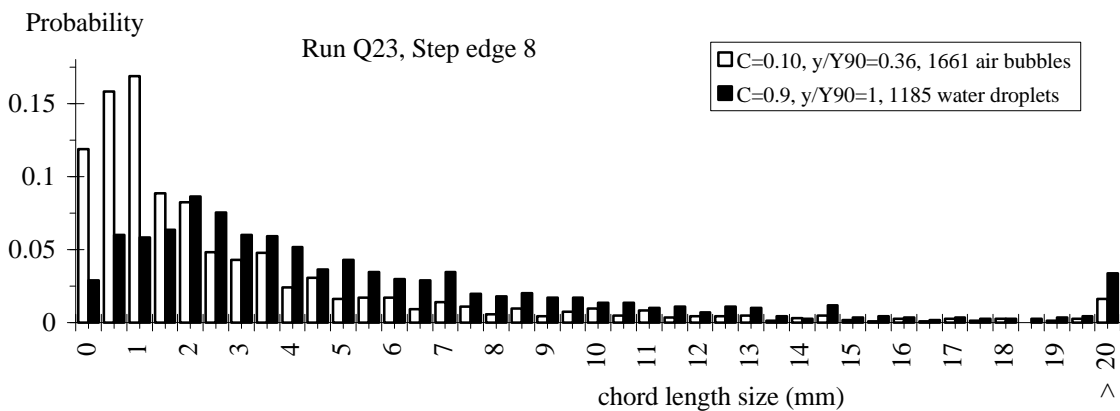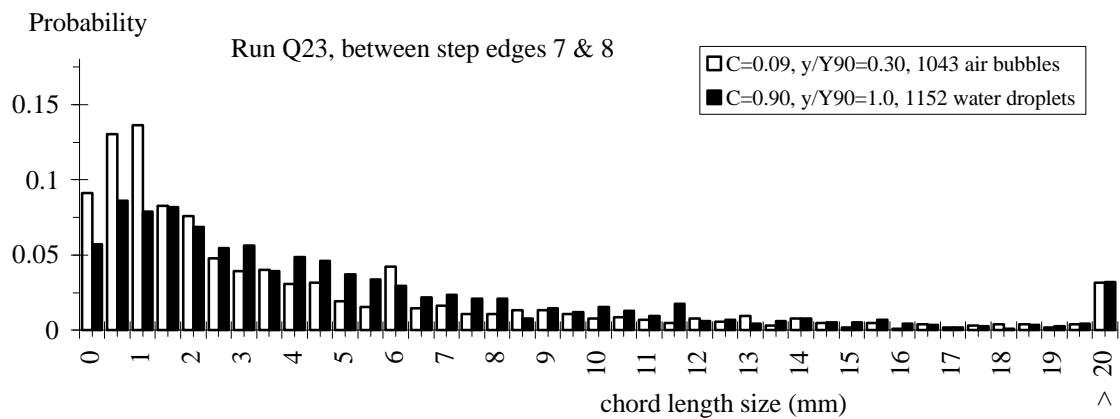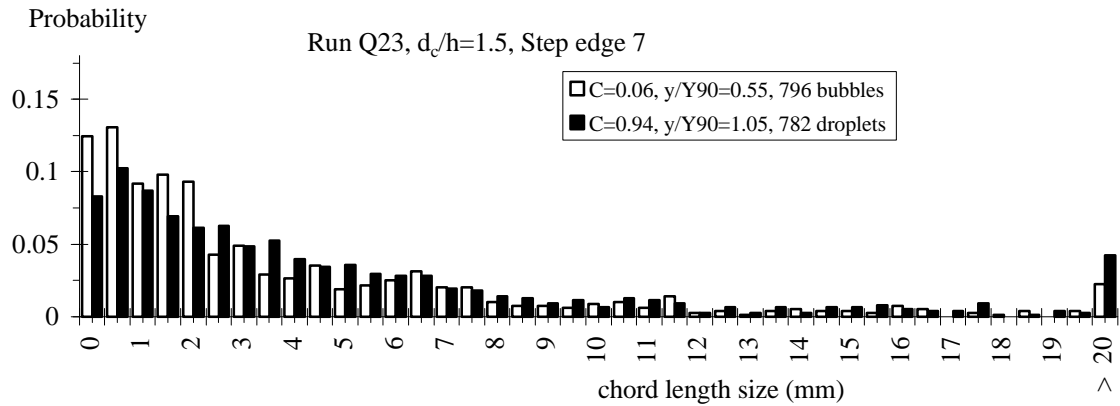
[2]No measurement was conducted in the recirculation cavity (y <0) to avoid probe tip damage.

(B) Void and liquid fractions : 20% ($Q_W = 0.114$ m^3/s)

	Y_{90} (m)	C_{mean}	$(F_{ab})_{max}$ (Hz)
Step edge 7	0.065	0.43	258
between step edges 7 and 8	0.070	0.53	205
Step edge 8	0.060	0.43	283

Run Q21, d_c/h=1.1, Step edge 7

□ C=0.17, y/Y90=0.39, 3567 bubbles
■ C=0.79, y/Y90=0.77, 2896 droplets

Run Q21, between step edges 7 & 8

□ C=0.26, Y/Y90=0.07, 1730 bubbles
■ C=0.8, y/Y90=0.86, 1358 droplets

Run Q23, Step edge 8

□ C=0.25, y/Y90=0.52, 2373 bubbles
■ C=0.78, y/Y90=0.76, 1993 droplets
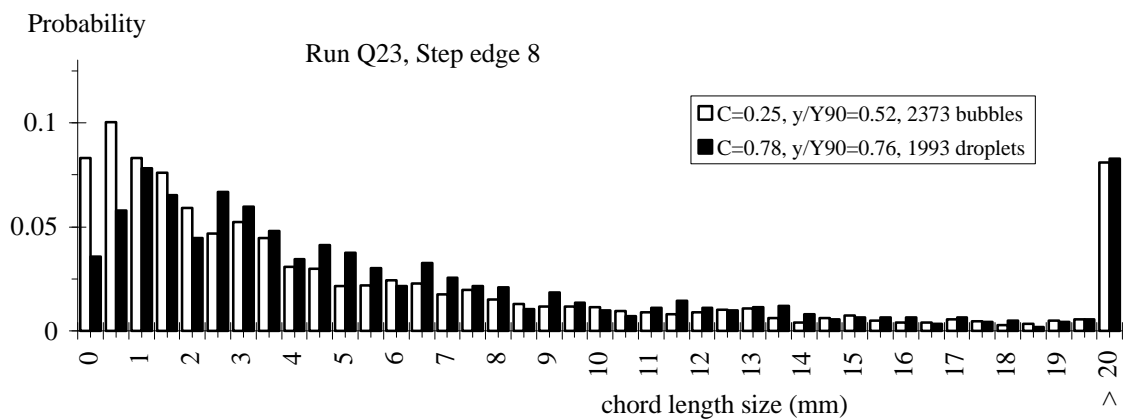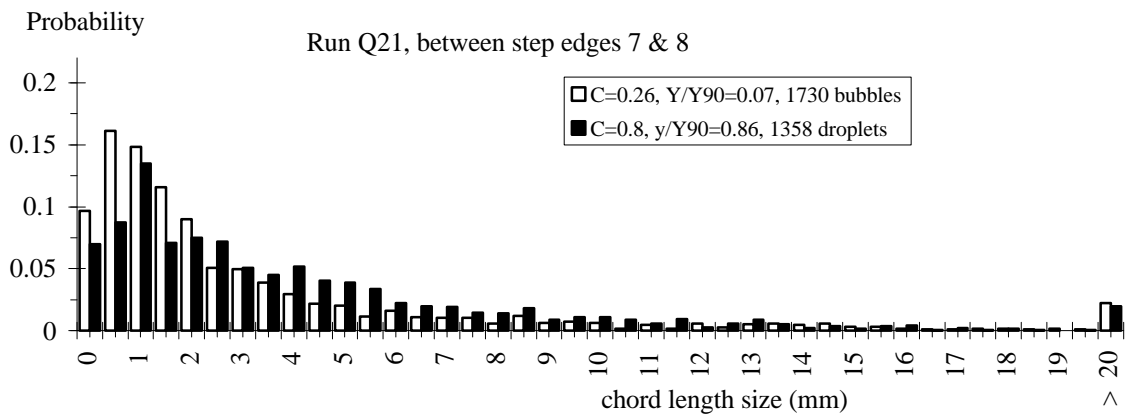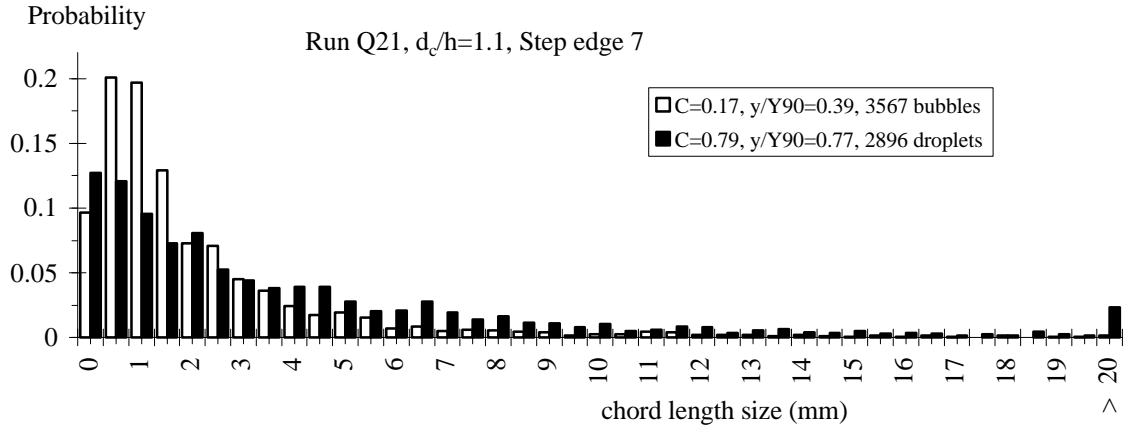
Turbulent velocity field

Distributions of time-averaged air-water velocity V and modified turbulence intensity Tu' are presented

in Figure 4-3. The data were measured with a dual-tip resistivity probe and details of the processing technique are given in Appendix IV. Although Tu' is not exactly equal to the turbulence intensity, it provides some qualitative information on the turbulence level in the flow. Figure 4-3B includes data measured at step edges (white symbols) and in between step edges (black symbols).

In Figure 4-3 the distributions of turbulence intensity Tu' exhibit relatively uniform profiles implying high turbulence levels across the entire air-water flow mixture (i.e. $0 \leq y \leq Y_{90}$). The trend differs significantly from well-known turbulence intensity profiles observed in turbulent boundary layers (e.g. SCHLICHTING 1979). On stepped chutes, it is believed that the high rate of energy dissipation, associated with form drag, contributes to strong turbulent mixing throughout the entire flow. Greater turbulence levels are expected within the developing shear layers : i.e. in the wake of each step edge. Despite some scatter, the trend is observed for the lower regions ($y/Y_{90} < 0.2$ to 0.3) (Fig. 4-3B).

Although the quantitative values of turbulence intensity Tu' are large (~ 100%), they are of the same order of magnitude as turbulence levels measured in separated flows past rectangular cavity (HAUGEN and DHANAK 1966, Fig. 9), in wakes between large stones (SUMER et al. 2001) and in the developing shear region of plunging water jets (CHANSON and BRATTBERG 1998).

Fig. 4-3 - Dimensionless velocity and turbulent intensity distributions in skimming flow
(A) $q_w = 0.182$ m^2/s, step edge 8
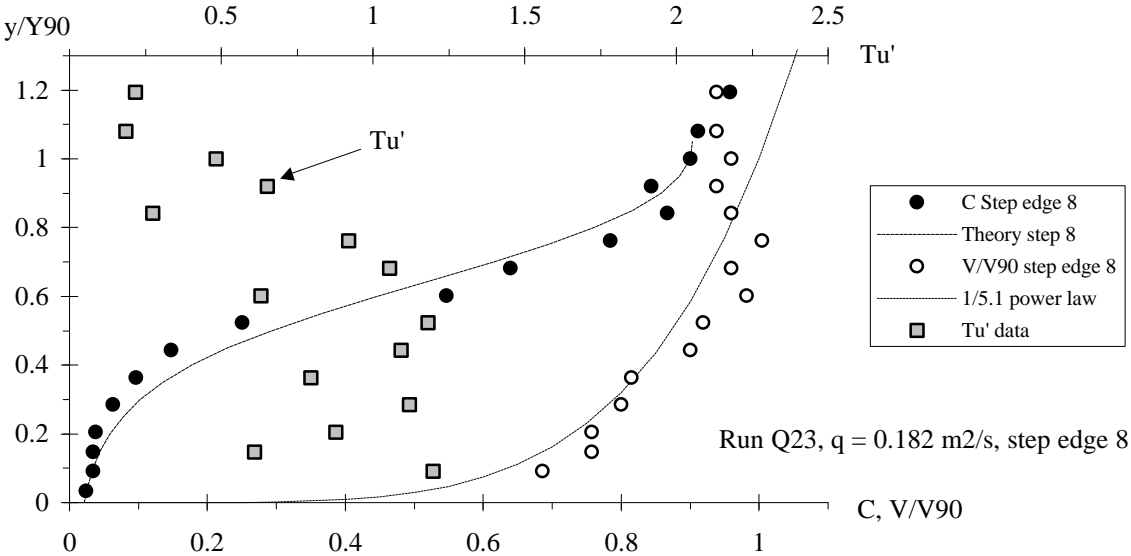
(B) Turbulent intensity distributions at step edges and in between step edges ($q_w = 0.182$ m^2/s)
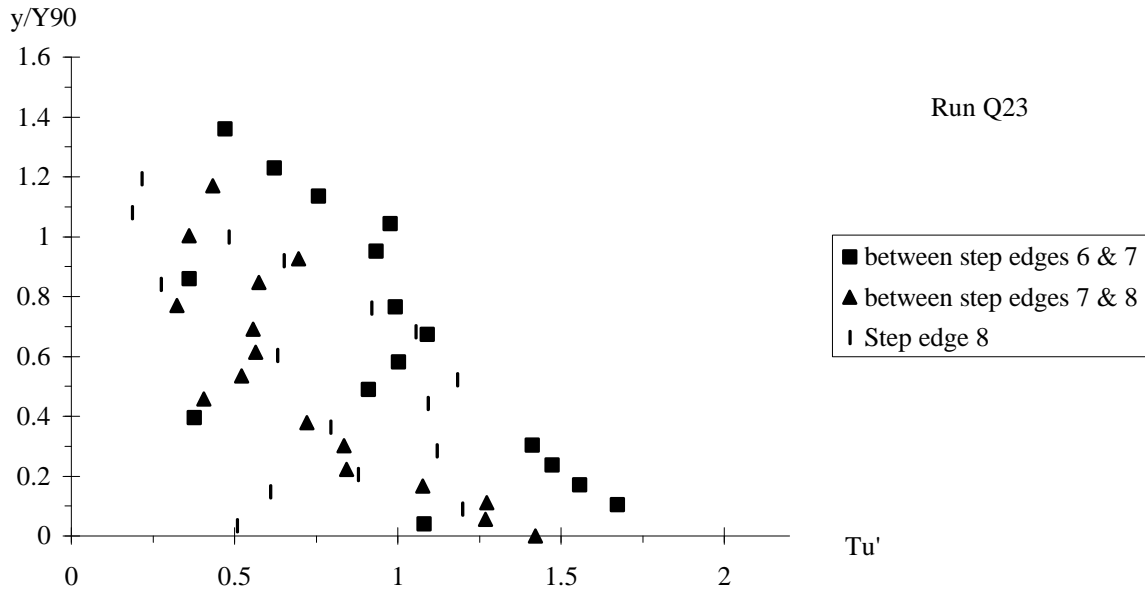
Comparison of void fraction profiles between smooth- and stepped-invert chute flows

Although the distribution of air concentration follows a trend similar to that seen in smooth-invert chute flows, small differences were consistently observed. This is highlighted in Figure 4-4 with a comparison of void fraction distributions obtained for identical mean air concentration. Black symbols are prototype smooth-invert chute data (CAIN 1978, Aviemore dam spillway) and the cross symbols are stepped chute data (Present study). The skimming flow data are compared with Equation (4-1) while smooth chute data are compared with CHANSON's (1995b) model developed and validated for smooth chute flows :

$$C \ = \ 1 \ - \ \tanh^2\!\left(K' \ - \ \frac{y/Y_{90}}{2 * D'}\right) \qquad\qquad \text{Self-aerated flows \ (4-4)}$$

where the integration constant K' and the dimensionless air bubble diffusivity D' are functions of the mean air content only (App. III).

The comparison of void fraction profiles indicates that, for an identical mean air content, skimming flows are more aerated in the upper flow layer (C > 0.3 to 0.5) than in smooth-invert self-aerated flows, and lesser air is observed in the lower layers (Fig. 4-4). A similar trend was observed with the stepped chute data of TOZZI et al. (1998). The result suggests a stronger droplet ejection mechanism in skimming flows, whereby water ejections reach comparatively higher elevations (than in smooth chute flows) before re-attaching to the flow. The trend may be related to different turbulent processes: i.e.,

24

skin friction in smooth-invert chutes versus form drag in skimming flow down stepped chutes.

Fig. 4-4 - Comparison of air concentration distributions in smooth-invert and stepped chute flows
Smooth-invert data : black symbols, solid line (Eq. (4-4))
Stepped chute date : cross symbols, dashed line (Eq. (4-1))
(A) $C_{mean} = 0.27$
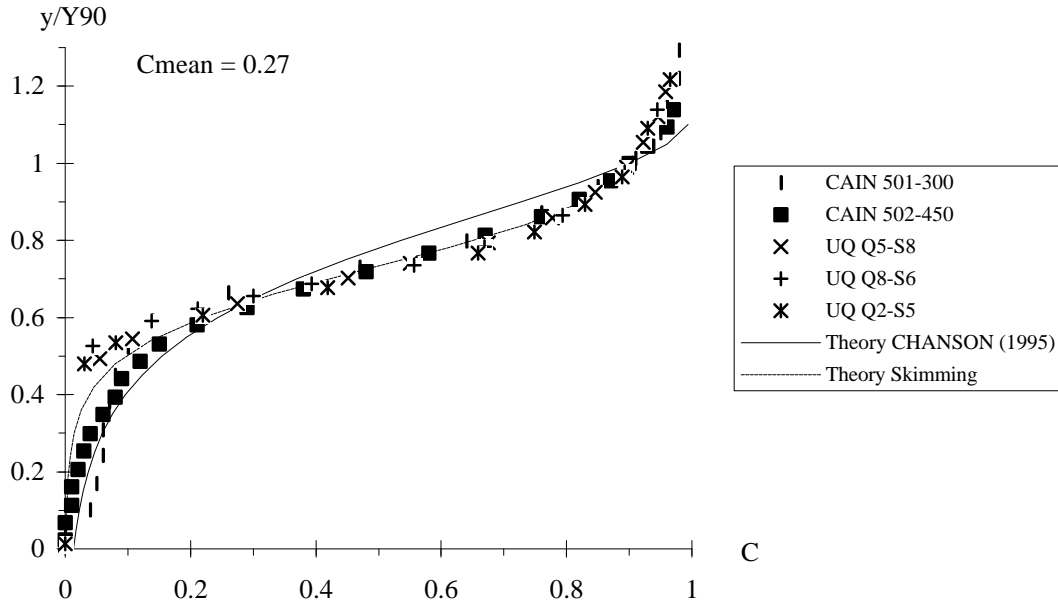
(B) $C_{mean} = 0.35$
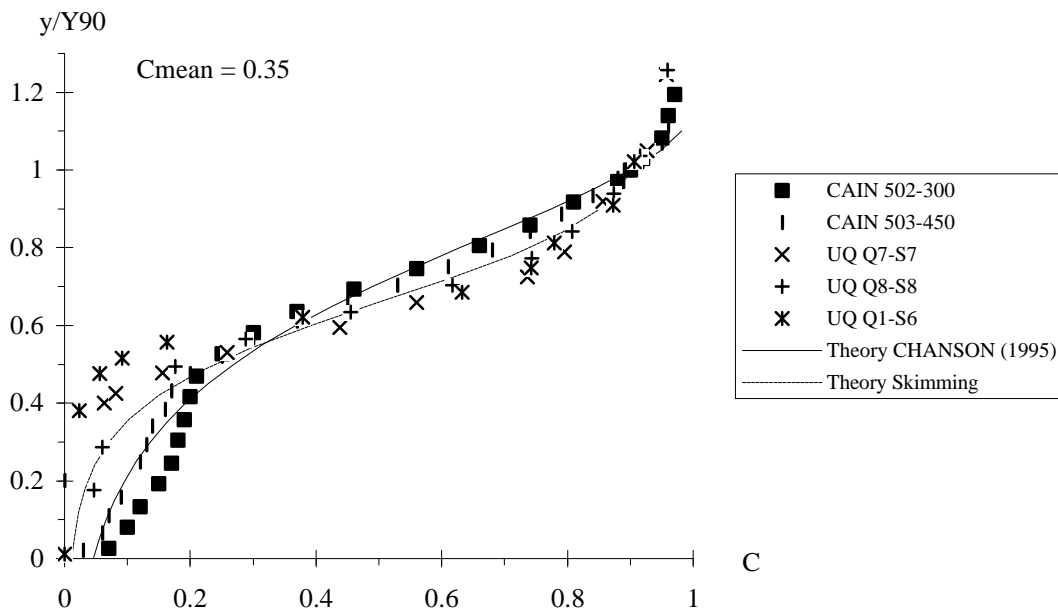
5. Air-water flow properties in transition flows

Free-surface aeration was found to be very intense for all transition flow rates (Table 2-1, App. I). Downstream of the inception point of free-surface aeration, mean air concentrations ranged from 0.2 to 0.6 typically, with maximum mean air content of up to 78% measured at one step edge. Major redistributions of air content and velocity were observed between adjacent, successive step edges. Similar longitudinal fluctuations of flow properties were observed in transition flows down a 3.4° stepped chute (h = 0.071 and 0.143 m) (CHANSON 2001), suggesting that the finding is not specific to the facility. Figure 5-1 shows air-water flow properties for one typical flow rate.

At most step edges, the distributions of air concentration may be fitted by :

$$C = K''' * \left(1 - \exp\left(- \lambda * \frac{y}{Y_{90}}\right)\right) \qquad \text{Transition flows} \quad (5\text{-}1)$$

where K''' and λ are function of the mean air content only (App. III). Equation (5-1) compares favourably with most data, except for the first step edge downstream of the inception point of free-surface aeration and for the deflecting jet flow (e.g. Fig. 5-1).

For most flow rates, a deflecting flow was observed a few steps downstream of the inception point of free-surface aeration. Visually, the flow appeared to bypass one step, barely touching the step edge. At that step, liquid fractions (1-C) greater than 10% were measured at distances up to $1.5*d_c$ and some spray overtopped the 1.25-m high sidewalls. The nappe re-attached the main flow at the next downstream step. In Figure 5-1A, such a deflected nappe is seen at the 6th step edge. (Further locations of deflected nappe are reported in Appendix I.)

In transition flows, the distributions of bubble count rates follow about the parabolic law (Eq. (4-3)) that was observed in smooth-invert chute flows and in skimming flows (Fig. 5-1B).

Turbulent velocity field

Air-water velocity distributions are presented in Figure 5-2 in terms of the time-averaged air-water velocity V and a modified turbulence intensity Tu' (Appendix IV). The distributions of turbulence intensity Tu' exhibit relatively uniform profiles across the air-water flow mixture (i.e. $y \leq Y_{90}$). The quantitative values of turbulence intensity Tu' are comparable with skimming flow data (Fig. 4-3).

The writers note that, in a transition flow, the shape of the air concentration profiles is nearly identical

for a given flow rate, while the velocity distributions are rapidly varied from step edge to step edge.

Discussion

Equation (5-1) is an analytical solution of the diffusion equation (App. III). It assumes that the air bubble diffusivity is zero for C = 0 and C = 1, and that it follows a distribution :

$$D' = \frac{C * \sqrt{1 - C}}{\lambda * (K' - C)} \tag{5-2}$$

The shape is somehow similar to the sediment diffusivity distribution developed by ROUSE (1937), leading to the Rouse distribution of suspended matter.

In a transition flow, the design of the sidewalls must account for the deflecting jet flows. That is, the chute sidewall height must be sized to at least $Y_{90} \sim 1.6 * d_c$, or even larger than $1.4 * Y_{90} = 2.2 * d_c$ if splashing is not acceptable : e.g., with a road next to the spillway chute and high risks of frost and icy conditions. For comparison, Y_{90}/d_c was found to be less than 0.7 to 0.8 in skimming flows, during the present study (Fig. 6-1A).

Fig. 5-1 - Experimental results in a transition flow
$Q_W = 0.058$ m^3/s - Comparison with Equation (5-1) - Inception point upstream of the step edge 3
(A) Air concentration and velocity distributions
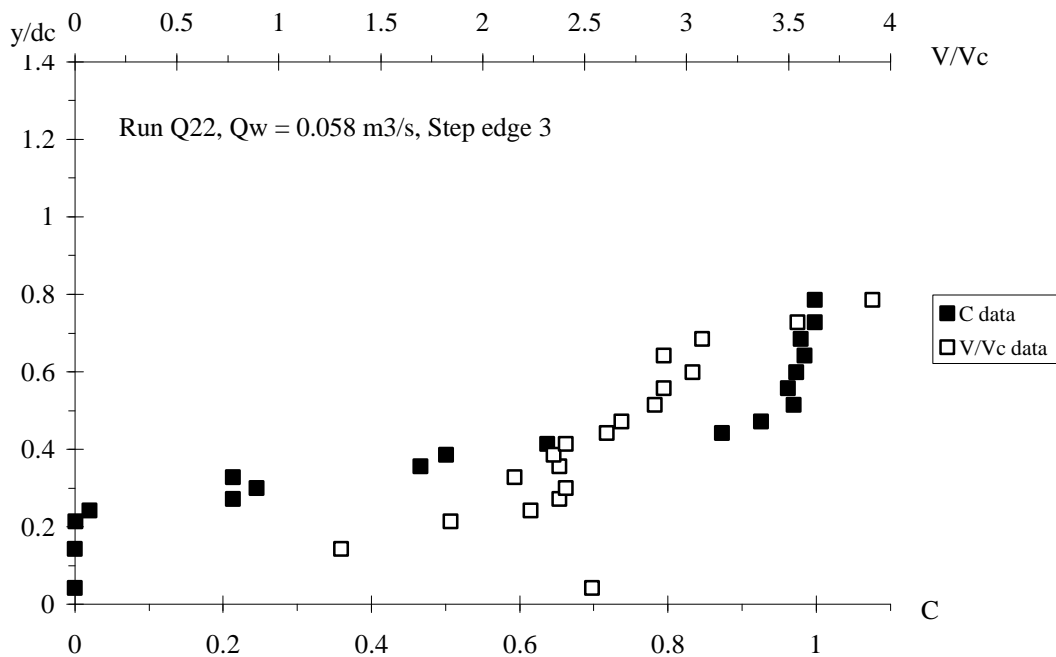
27

(A) Air concentration and velocity distributions

Run Q22, Qw = 0.058 m3/s, Step edge 4

Run Q22, Qw = 0.058 m3/s, Step edge 5

(A) Air concentration and velocity distributions

Run Q22, Qw = 0.058 m3/s, Step edge 6
Deflecting nappe

Run Q22, Qw = 0.058 m3/s, Step edge 7
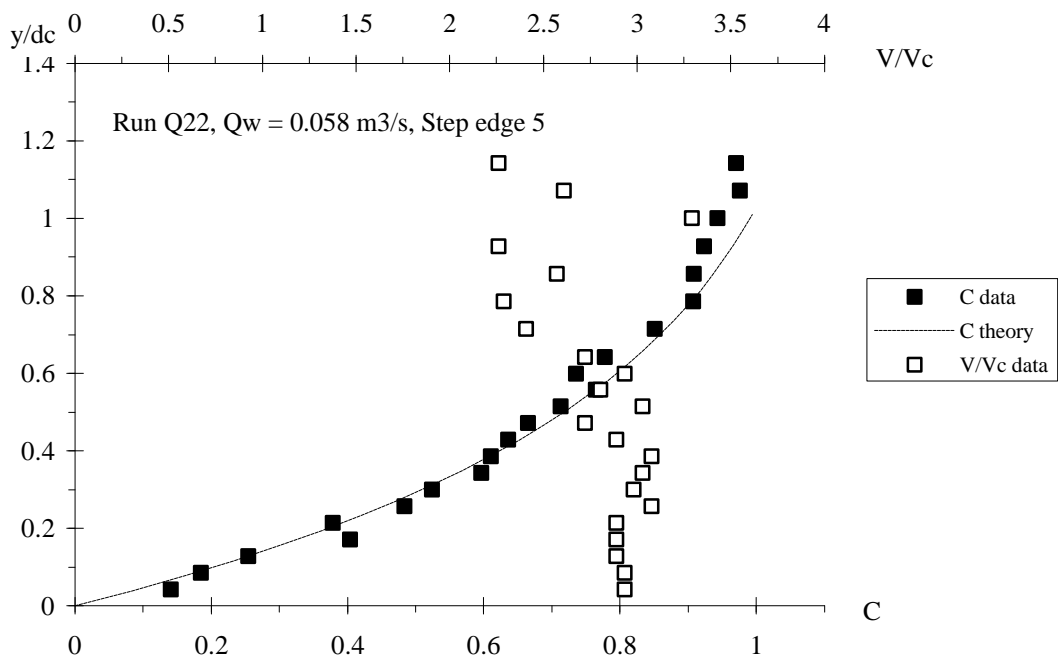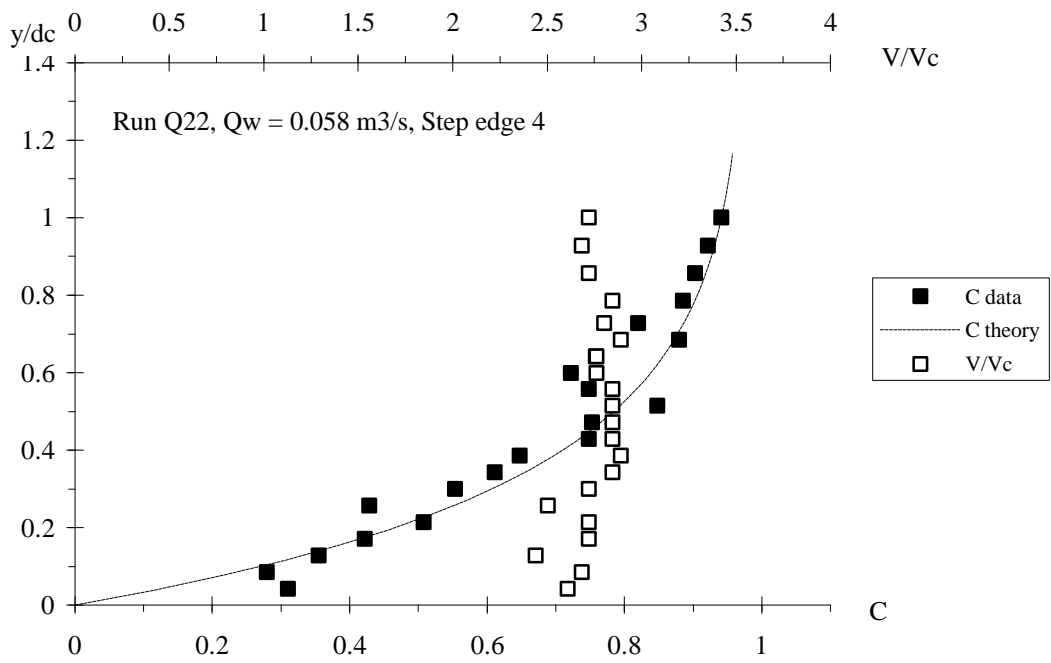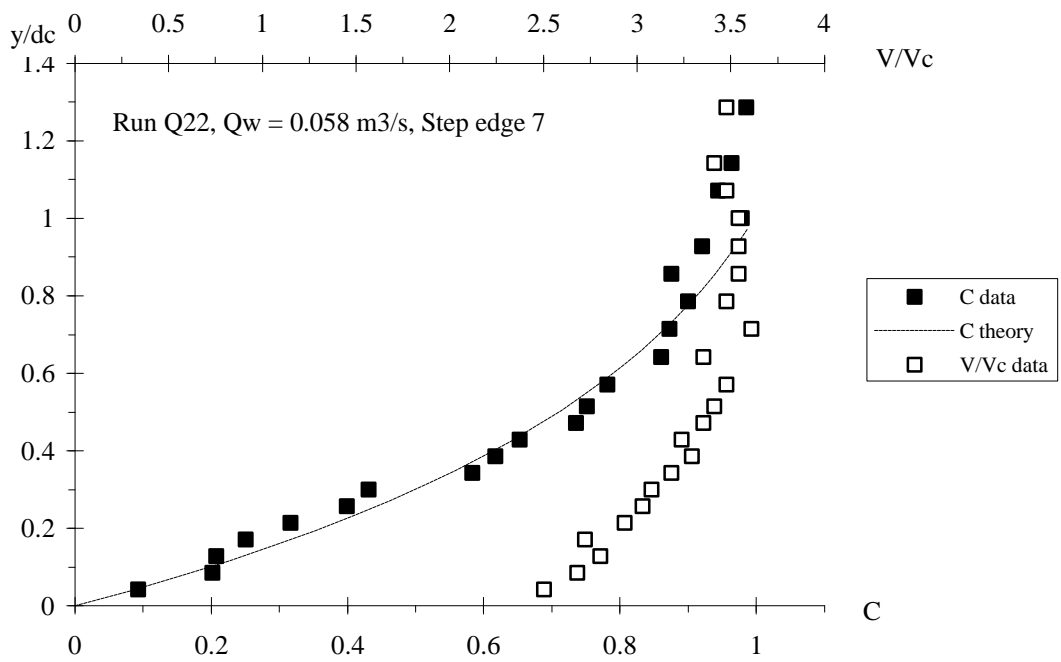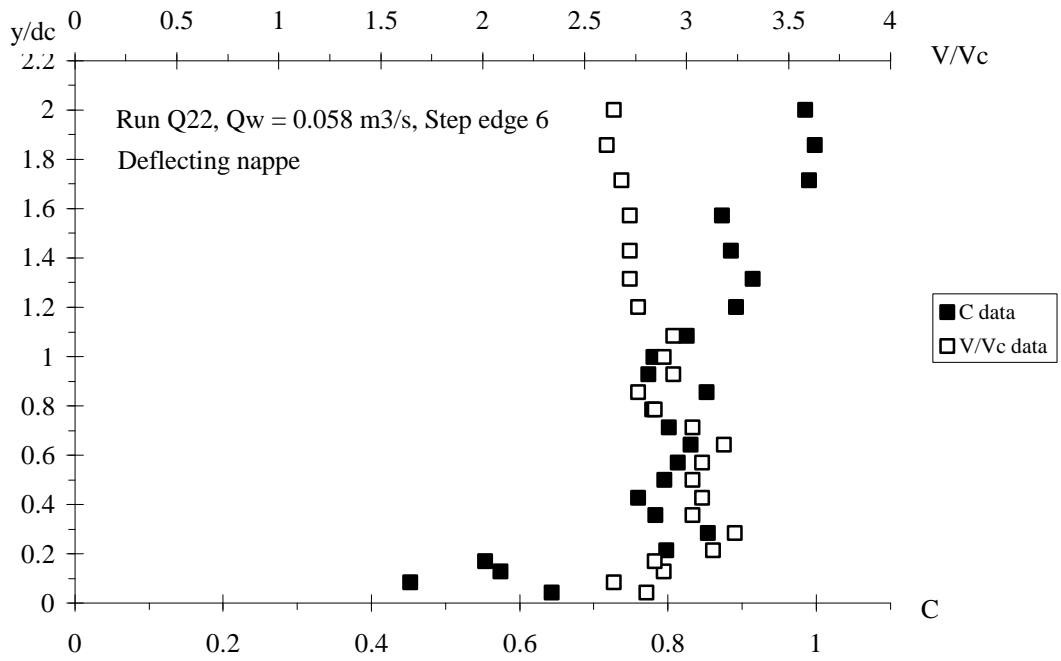
(A) Air concentration and velocity distributions
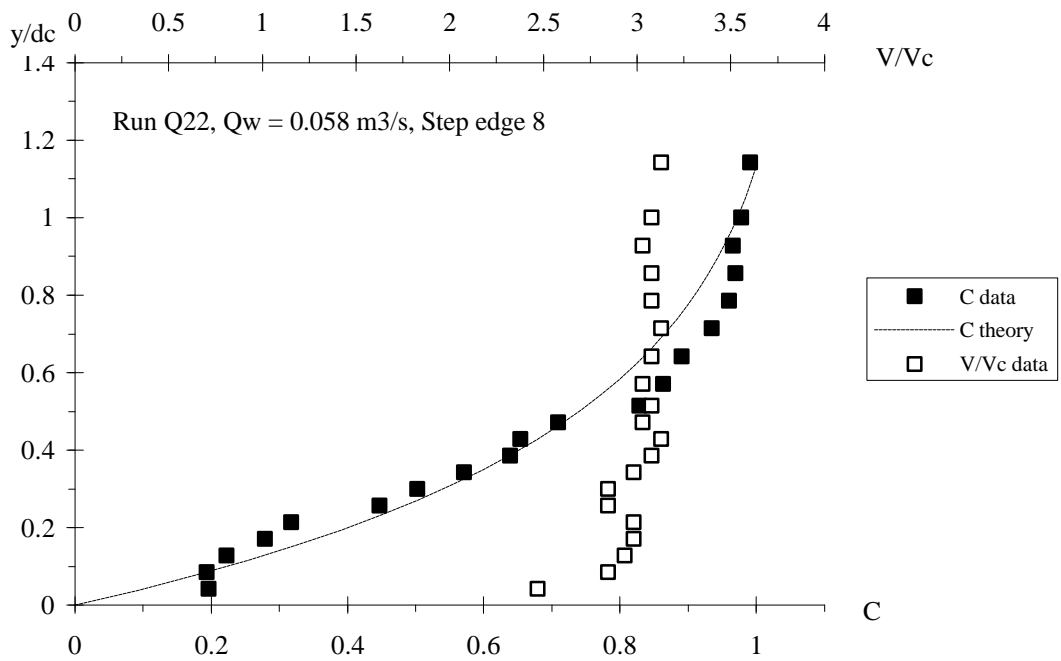
(B) Dimensionless bubble count rate distributions
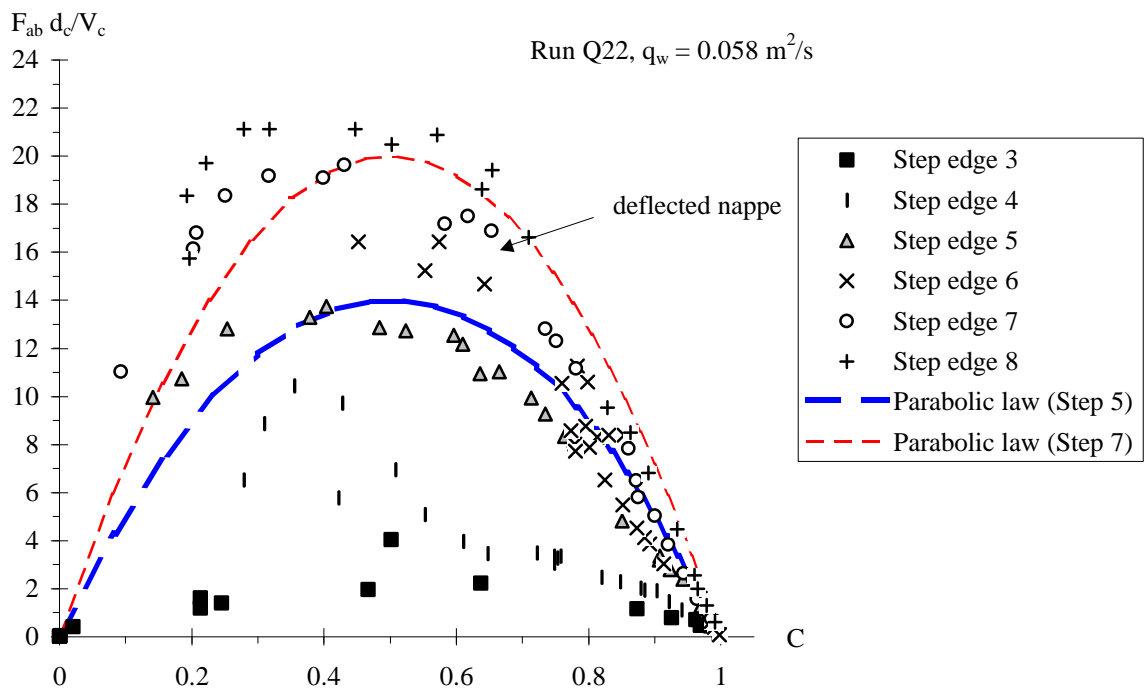
Fig. 5-2 - Dimensionless velocity and turbulent intensity distributions in transition flow
Run Q22, $q_w = 0.058$ m^2/s, step edge 8
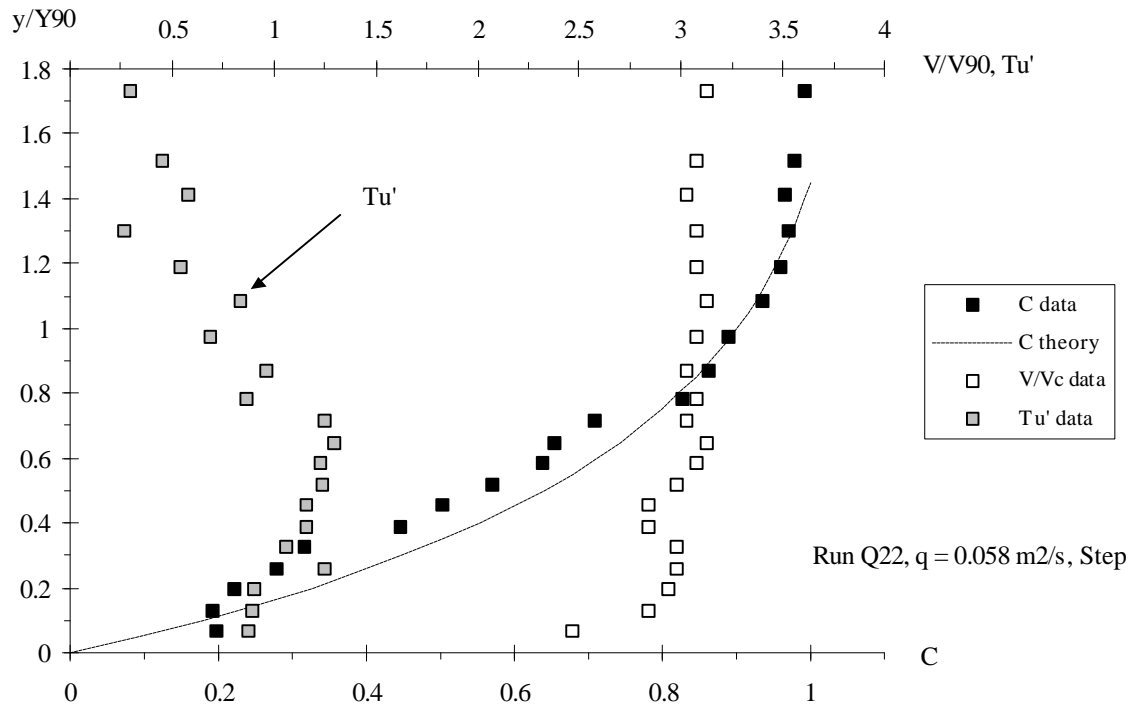
6. Discussion : air-water flow properties and flow resistance

6.1 Air-water flow properties

Longitudinal distributions of mean air concentration C_{mean} and dimensionless air-water depth Y_{90}/d_c are presented in Figure 6-1, where the horizontal axis s/d_c is the ratio of the distance from the downstream end of the broad crest to the critical depth. Note that the chute was relatively short and that uniform equiibrium flow conditions were not achieved at the downstream end.

In skimming flows, rapid aeration was observed at the inception point, followed by a gradual increase (Fig. 6-1A). In Figure 6-1A, the data are compared with the numerical model developed for smooth-invert chutes by WOOD (1985) and extended by CHANSON (1993b). Calculations were conducted assuming a friction factor f = 0.3.

Transition flow data are presented in Figure 6-1B. Note the different horizontal and vertical ranges between Figures 6-1A and 6-1B. Very large aeration was observed in transition flows, in excess of acknowledged limits observed in smooth chute flows (e.g. WOOD 1991, CHANSON 1997b,c). The air-water flow depth data Y_{90} exhibited a saw-edged pattern, reaching up to 1.4 to 1.6 times d_c at

deflected nappes. Overall both sets of curves do not show a monotonic trend. Rather chaotic, irregular

variations with increasing distances from the crest were observed.

Fig. 6-1 - Longitudinal distributions of mean air content C_{mean} and dimensionless depth Y_{90}/d_c
(A) Skimming flow data - Comparison with numerical calculations (WOOD 1985, CHANSON 1993b)
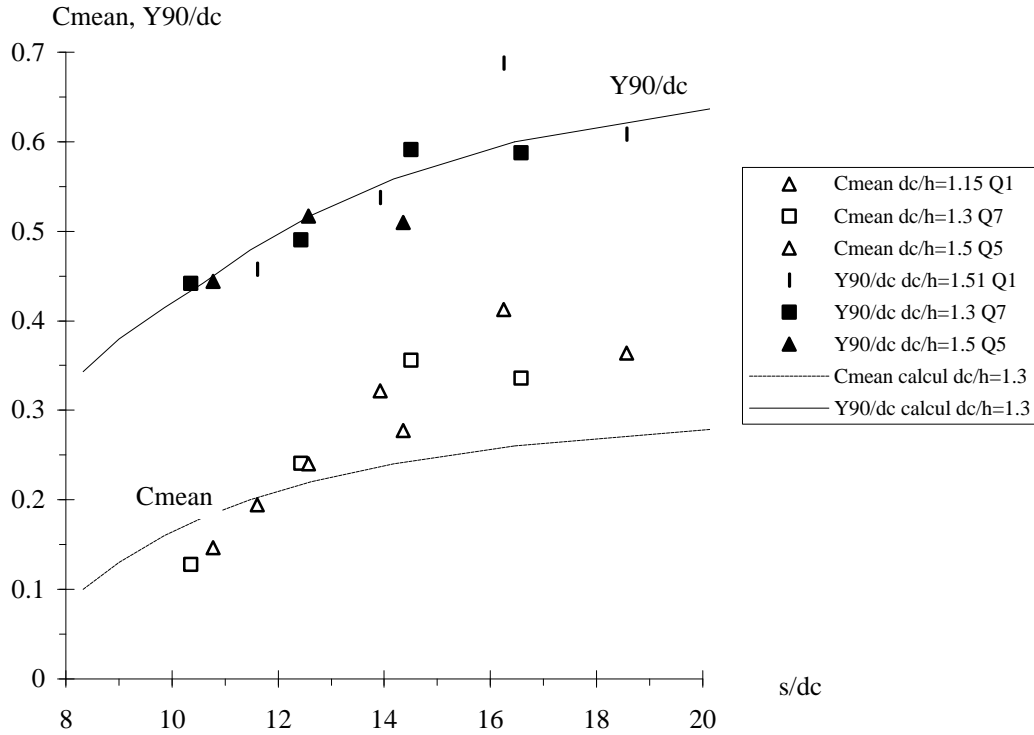
(B) Transition flow data
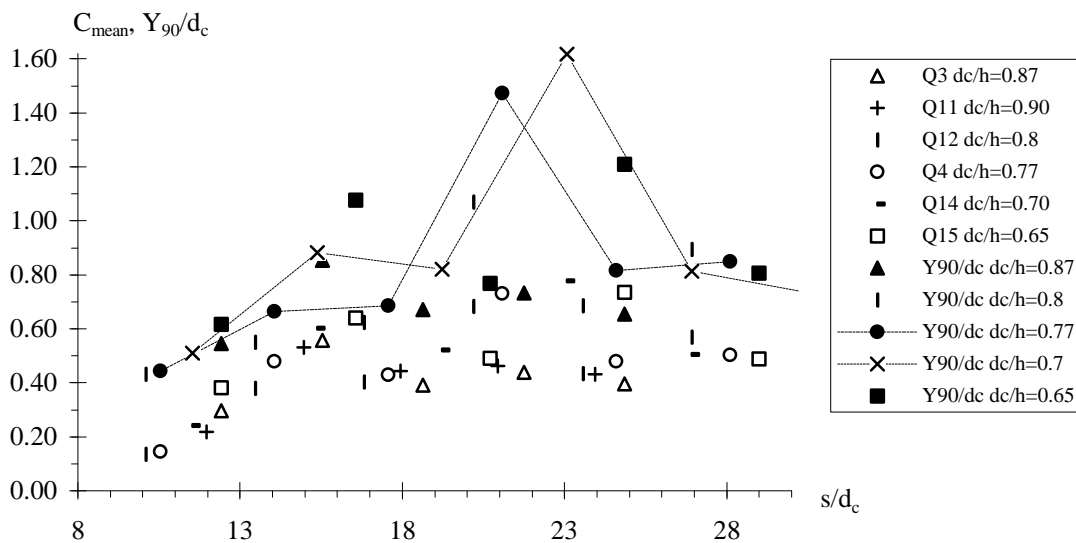
Similar instabilities were measured down a 3.4º stepped chute (h = 0.07 & 0.14 m) at the University of Quensland (CHANSON 2001). OHTSU and YASUDA observed also the chaotic nature of transition flows for slopes ranging from 5.7º to 55º, although it appeared more pronounced "cha os" for $\alpha < 35º$ (Personal communication).

Experimental results show that the maximum bubble frequency $(F_{ab})_{max}$ increased with longitudinal distance for each and every flow rate, and that it did not reach an upper limit within the length of the experimental channel. The test section was indeed relatively short and uniform equilibrium was not achieved at the downstream end. Figures 4-1C and 5-1B illustrate the longitudinal increase in maximum bubble frequency for a skimming flow and a transition flow respectively.

6.2 Flow resistance in skimming flows

Skimming flows are characterised by significant form drag and form losses take place predominantly in the cavity recirculation (see section 3.2, App. II). In gradually-varied flows downstream of the inception point, the average shear stress between the skimming flow and the cavity recirculation may be calculated from the friction slope S_f [3]. For a wide channel the energy equation yields:

$$f_e = \frac{8 * \tau_o}{\rho_w * U_w^2} = \frac{8 * g * \left(\int_{y=0}^{y=Y_{90}} (1 - C) * dy \right) * S_f}{U_w^2} \qquad \text{Gradually-varied flow (6-1)}$$

where the friction slope equals $S_f = - \partial H/\partial s$, H is the depth-averaged total head, s is the curvilinear coordinate along the flow direction, f_e is the Darcy friction factor for air-water flow, C is the local void fraction, y is measured normal to the pseudo-invert formed by the step edges, and U_w is the mean flow velocity $(U_w = q_w/d)$. For the present series of experiments, the flow resistance was estimated using Equation (6-1) (Table 6-1). In Figure 6-2, the data are compared with experimental data obtained in large-size laboratory flumes : i.e., h > 0.02 m and Re > 1 E+5. All 166 data were re-analysed using the criteria of CHANSON et al. (2000).

0.30 (166 data) (Fig. 6-2B).

---

[3]The friction slope is the slope of the total head line (HENDERSON 1966, CHANSON 1999b).

Table 6-1 - Summary of experimental results of flow resistance in skimming flows

Ref.	Q_w m^3/s	Flow regime	f_e	Remarks
(1)	(2)	(3)	(3)	(4)
Series 1				Single-tip probe.
	0.182	Skimming flow	0.143	Run Q5
	0.164	Skimming flow	0.157	Run Q6
	0.147	Skimming flow	0.196	Run Q7
	0.130	Skimming flow	0.184	Run Q8
	0.124	Skimming flow	0.215	Run Q1
	0.114	Skimming flow	0.283	Run Q9
	0.103	Skimming flow	0.157	Run Q2
	0.099	Transition flow	0.158	Run Q10
Series 2				Double-tip probe.
	0.182	Skimming flow	0.092	Run Q23.
	0.114	Skimming flow	0.074	Run Q21.

Fig. 6-2 - Flow resistance in skimming flow: conditional analysis
(A) Steep stepped chute data ($\alpha > 20°$) {166 data} - Comparison with Equation (6-2) ($f_d = 0.2$)
Laboratory data :

f_i (estimate neglecting air entrainment)	BaCaRa (1991), YASUDA and OHTSU (1999), SHVAINSHTEIN (1999)
f_e (based upon air-water flow properties)	CHAMANI and RAJARATNAM (1999), YASUDA and OHTSU (1999) (55° only), MATOS (2000), BOES (2000), Present study
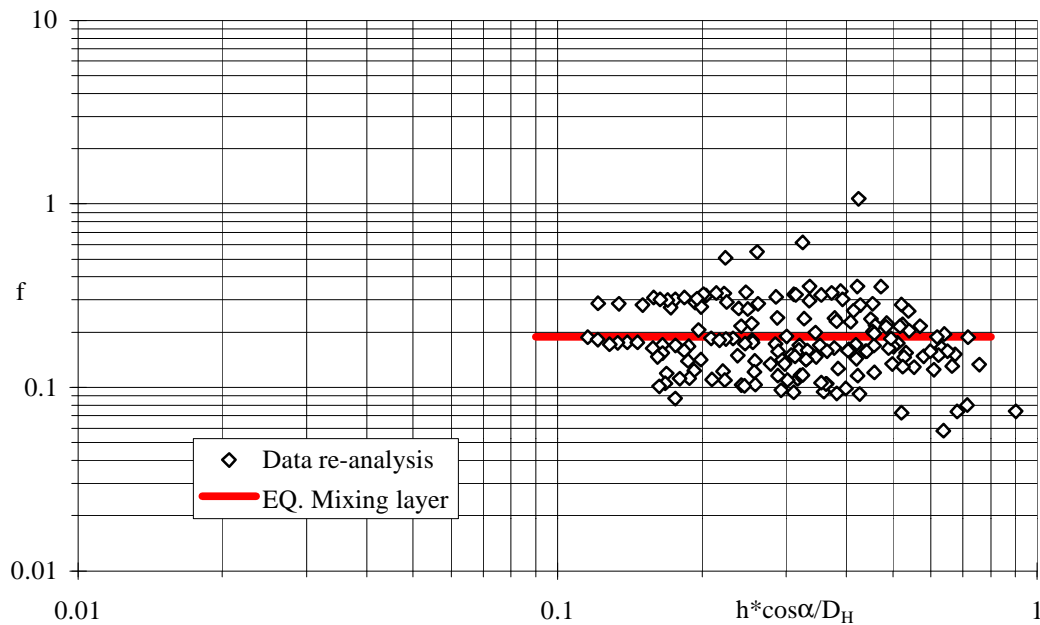
(B) Probability distribution function of steep chute friction factor ($\alpha > 20°$) {166 laboratory data}

f_i (estimate neglecting air entrainment)	BaCaRa (1991), YASUDA and OHTSU (1999), SHVAINSHTEIN (1999)
f_e (based upon air-water flow properties)	CHAMANI and RAJARATNAM (1999), YASUDA and OHTSU (1999) (55° only), MATOS (2000), BOES (2000), Present study

Uncontrolled broad-crest	YASUDA and OHTSU (1999), Present study
Uncontrolled smooth ogee crest	CHAMANI and RAJARATNAM (1999)
Uncontrolled ogee crest, with small first steps in ogee development	BaCaRa (1991), SHVAINSHTEIN (1999), MATOS (2000)
Pressurised intake	BOES (2000)
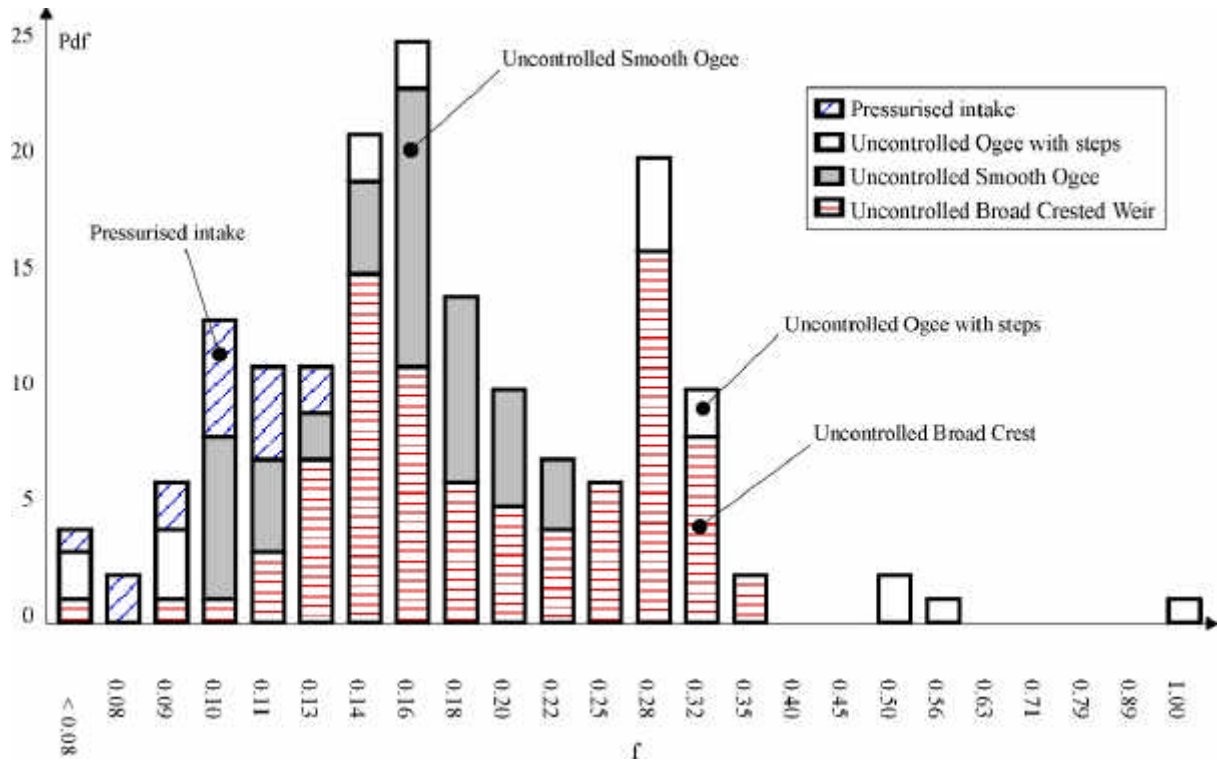
The friction factor data present no obvious correlation with the relative step roughness ($h*\cos\alpha/D_H$), Reynolds, Froude nor Weber numbers. However they compare favourably with a simplified analytical model of the pseudo-boundary shear stress which may be expressed, in dimensionless form, as :

$$f_d = \frac{8 * \tau_o}{\rho_w * U_w^2} = \frac{2}{\sqrt{\pi}} * \frac{1}{K} \tag{6-2}$$

where f_d is an equivalent Darcy friction factor estimate of the form drag, $1/K$ is the dimensionless expansion rate of the shear layer (CHANSON et al. 2000). Equation (6-2) predicts $f_d \approx 0.2$ for $K = 6$: i.e., close to the observed friction factors (Fig. 6-2A).

Figure 6-2B presents the probability distribution function of the Darcy friction factor where the

histogram columns represent the number of data with friction factors within the interval ([4]) : e.g., the probability of friction factors from 0.18 to 0.20 is represented by the column labelled 0.18. The first and last column indicates the number of data with friction factors less than 0.08 and greater than 1.0 respectively. The experimental data are distributed around three dominant values: $f \approx 0.105$, 0.17 and 0.30 (166 data) (Fig. 6-2B).

Fig. 6-3 - Cavity recirculation, developing shear layer and re-attachment in skimming flows
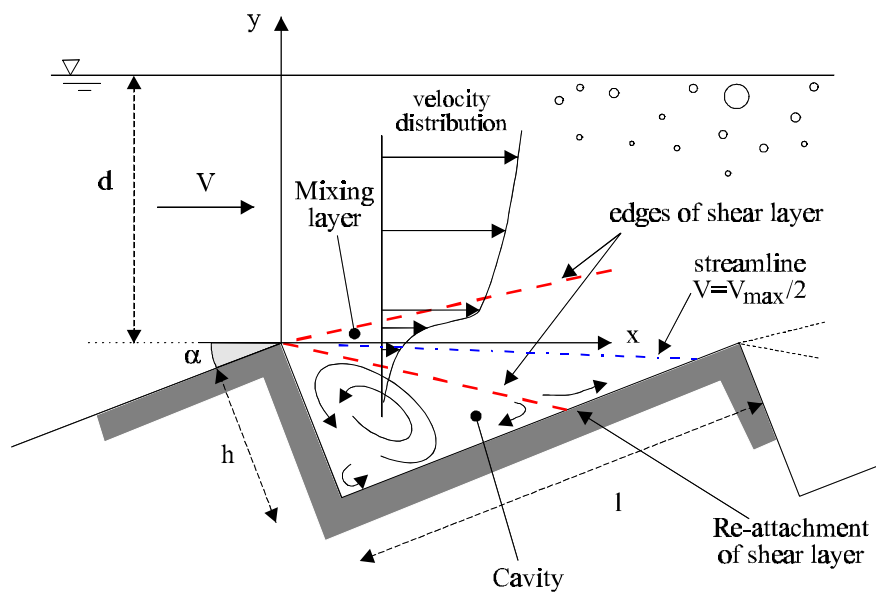
Discussion

The writers hypothesise that flow resistance in skimming flows (down steep slopes) is not an unique function of the flow rate and stepped chute geometry, but that the form drag process presents several modes of excitation. At each step edge, shear instabilities may develop in the shear layer (e.g. NAUDASCHER 1967) (Fig. 6-3). In turn, the instabilities could generate different cavity wake regimes, associated with different drag coefficients. In Figure 6-2B, the dominant values $f \approx 0.105$, 0.17 and 0.30 are assumed to correspond to the three dominant modes (or regimes).

Different modes of excitation may be induced by different inflow conditions, affecting cavity recirculation processes in a cascading effect (i.e. sequential cavity ejections, Fig. 3-3). At the upstream

---

[4]The intervals were selected with a constant logarithmic increment

end, the inflow turbulence does affect the cavity recirculation and the distance to re-attachment of the shear layer (Fig. 6-3). In turn, this will affect all the stepped chute because of the sequential ejection process (Fig. 3-3). Figure 6-4 summarises basic inflow configurations. With an uncontrolled ogee profile, the pressure distribution is atmospheric in the entire flow at design flow conditions by definition of the ogee development (HENDERSON 1966, CHANSON 1999b) ([5]). The inflow pressure coefficient C_p is zero, where C_p is defined as :

$$C_p \;=\; \frac{1}{\frac{1}{2} * \rho * g * d^2} * \int_0^d P(y) * dy$$

With an uncontrolled broad-crest, the pressure is hydrostatic at the crest and $C_p = 1$. For a pressurised intake, the inflow pressure distribution is greater than hydrostatic (i.e. $C_p \gg 1$).

Figure 6-2B shows that experiments with pressurised intake yield lower flow resistance than for uncontrolled inflow conditions. For example, the re-analysis of BOES' (2000) data gives f ~ 0.1 : i.e., about three times smaller than the third dominant value. Skimming flow experiments at the University of Queensland down a flat slope (α = 3.4º, h = 0.07 m) yielded friction factors f ~ 0.03, that are three times smaller than data of YASUDA and OHTSU (1999) (f ~ 0.08) on a 5.7° stepped slope (h = 0.025 & 0.05 m) with uncontrolled broad-crest.

The type of excitation mode (or regime) may further be affected by the cavity dimensions (ratio h/l), cavity aeration (greater aeration are likely on steep slopes), and compliance of the stepped invert (construction material) which could lead to different vibration regimes. There is some analogy with form drag behind bluff bodies. For the flow behind a cylinder, the drag coefficient is known to be a function of the upstream turbulence affecting the boundary layer separation for a given Reynolds number ([6]). For ventilated cavities behind wedges and wings, several regimes were associated with different drag coefficients for the same inflow conditions, depending upon the amount of ventilation (SILBERMAN and SONG 1961, LAALI and MICHEL 1984, MICHEL 1984, VERRON and

---

[5]A further sub-division may be made between an entire smooth ogee profile and an ogee development with small first steps in the profile (Fig. 6-3).

[6]For infinitely long smooth cylinders, the effect is best observed for Reynolds numbers about 1 E+5 to 1 E+6.

MICHEL 1984).

The above results may further be influenced by drag reduction associated with air bubble entrainment (section 6.3).

Fig. 6-4 - Definition sketch of inflow conditions
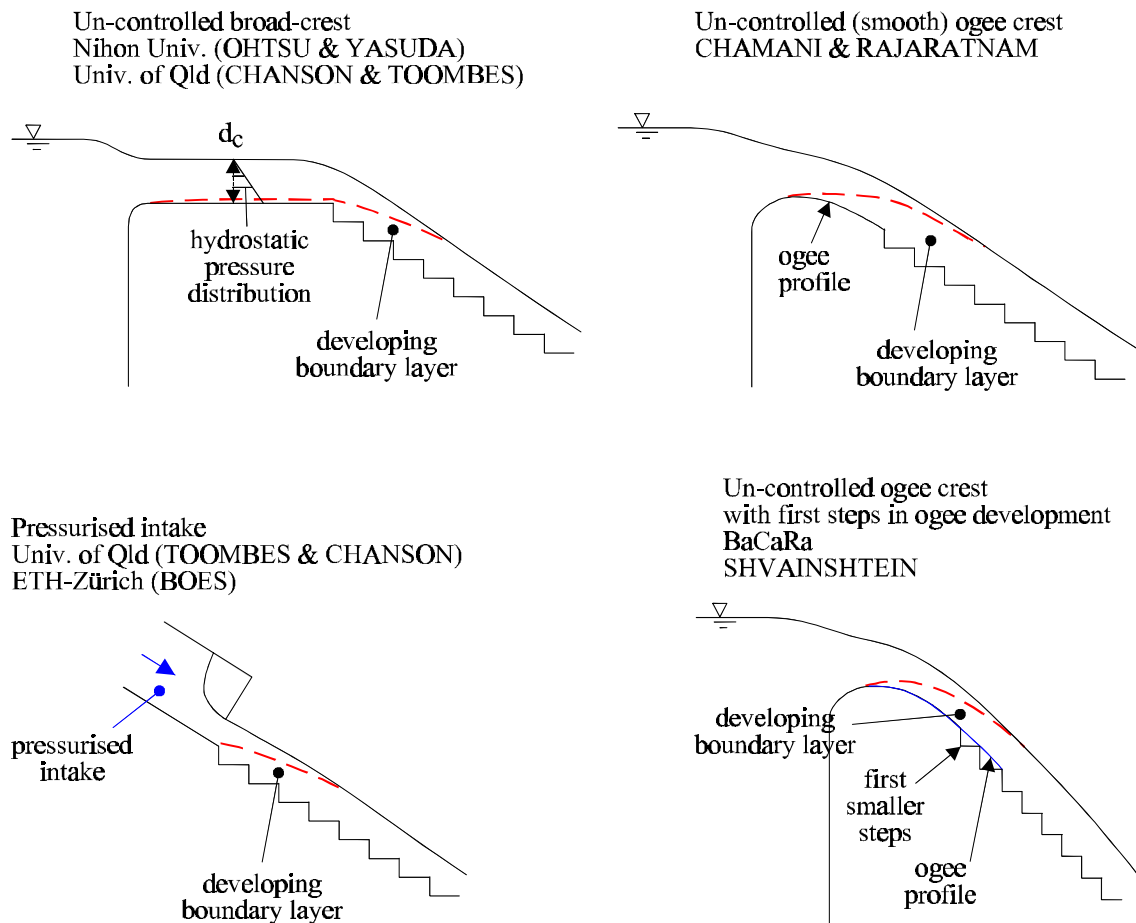
6.3 Drag reduction in skimming flows

On smooth-invert chutes, the presence of air within turbulent boundary layers reduces the shear stress between flow layers, and hence the shear force (WOOD 1983, CHANSON 1994). An estimate of the drag reduction is :

$$\frac{f_e}{f} = 0.5 * \left(1 + \tanh\left(0.628 * \frac{0.514 - C_{mean}}{C_{mean} * (1 - C_{mean})} \right) \right) \qquad \text{Smooth chute (6-3)}$$

where tanh is the hyperbolic tangent function, C_{mean} is the mean air concentration, f is the clear-water friction factor and f_e is the Darcy friction factor of air-water flow (CHANSON 1994). Equation (6-3)

characterises the reduction in skin friction associated with air entrainment causing a thickening of the momentum sublayer (CHANSON 1994,1997b).

The re-analysis of detailed air concentration measurements in skimming flows shows a decrease in friction factor f_e with increasing mean air concentration (Fig. 6-5, Table 1-1). The re-analysed stepped chute data are best correlated by :

$$\frac{f_e}{f_d} = 0.5 * \left(1 + \tanh\left(0.68 * \frac{0.5 - C_{mean}}{C_{mean} * (1 - C_{mean})} \right) \right) \qquad \text{Skimming flow (6-4)}$$

where f_d is the dimensionless pseudo-boundary shear stress for clear-water flow (Eq. (6-2)). Equation (6-4) is compared with experimental data in Figure 6-5 assuming a mixing layer expansion rate : $1/K = 0.22$ (Eq. (6-2)). Equation (6-3) is also shown. Despite some scatter, the results confirm CHANSON's assumption that a drag reduction process caused by air entrainment occurs on stepped spillways (CHANSON 1993a,1995a). The trend (Eq. (6-4)) is very close to drag reduction estimate on smooth-chutes (Eq. (6-3)) although the drag reduction mechanism is entirely different (Fig. 6-5).

In skimming flows, separation occurs at each step edge and a shear layer develops with cavity recirculation beneath (Fig. 3-3 & 6-3). It is believed that drag reduction results from interactions between the entrained bubbles and the developing mixing layer. Small air bubbles tend to resist stretching and this leads to some vortex inhibition. Hydrodynamic interactions between bubbles affect their orientation in the flow and might play a key role in reducing the instability of the flow as with fibre addition in water flows (e.g. AZAIEZ 2000). Interactions between particles and turbulent structures were visualised in developing shear layers of dilute polymer solutions, showing the existence of large-scale turbulent structures and a drastic reduction in number of small-scale eddies with polymer additives (e.g. RIEDIGER 1989).

Fig. 6-5 - Drag reduction in skimming flows - Comparison between Equations (6-3) and (6-4), and

laboratory data

f_e (based upon air-water flow properties)	CHAMANI and RAJARATNAM (1999), YASUDA and OHTSU (1999) (55° only), MATOS (2000), BOES (2000), Present study